

The effect of navigation on river dunes

Master's Thesis
Civil Engineering & Management



Paul Bongers
September 2021



Rijkswaterstaat
Ministerie van Infrastructuur en Waterstaat

**UNIVERSITY
OF TWENTE.**

Colophon

Title: The effect of navigation on river dunes
Author: Ing. P.S.J. (Paul) Bongers
Student number: 2216744
Version: Final
Date: September 26, 2021
Institution: University of Twente
Master: Civil Engineering and Management
Master programme: River and Coastal Engineering

Head of committee: Prof. dr. S.J.M.H. (Suzanne) Hulscher
Internal supervisor: Dr. J.J. (Jord) Warmink
Daily supervisor: Ir. L.R. (Lieke) Lokin
External supervisor: Ir. M.C. (Merel) Verbeek
External supervisor: Ing. B.M.A.J. (Brian) Vrijaldenhoven

Figure on cover page: The Waal at Boven-Leeuwen (Van Elk, 2018)

Preface

Before you, lies the thesis “Effect of navigation on river dunes”. The research was conducted for Rijkswaterstaat ON. The thesis has been written to fulfil the graduation requirements of the Civil Engineering and Management master at the University of Twente. The research has been carried out from February 2021 until September 2021.

First, I would like to thank my external supervisors Brian and Merel from Rijkswaterstaat ON for their guidance, insights and support. Despite the obligations that everything had to be digital, they really made the best of it. Secondly, I would like to thank my internal supervisors Lieke, Jord and Suzanne for their guidance and feedback. Especially, my internal daily supervisor Lieke was always willing to help and she gave me many new insights during the process. Thirdly, I would like to thank my family and friends for their support throughout my thesis.

Paul Bongers

Enschede, September 2021

Summary

The sand bed in the Waal river is characterised by river dunes. The hypothesis is that river dunes become normative for the navigation depth during low water if sufficient water depth is created at five local spots with the least water depth (in Dutch: Minst Gepeilde Dieptes). These local spots do not erode uniformly with the rest of the river bed due to the presence of the fixed layers. Water movement induced by navigation affects the geometry and celerity of the river dunes. The aim of this research is, therefore, to quantify this potential effect of navigation on the geometry and celerity of the river dunes to improve river bed management.

For this research, the study area in the Waal near Druten was chosen because of the minimal effect of river interventions and bend processes and no tidal influence. Navigation has the most impact on the river bed during low water. The correct low water conditions were observed during the selected time periods 2019-07-19 – 2019-10-14 and 2020-07-10 – 2020-09-21. These selected time periods had an average water level of 4.53 m + NAP (2019) and 4.26 m + NAP (2020) at Druten.

The MultiBeam Echo Soundings data contained the bed level measurements of the Waal. Wavelet analysis with the Morlet wavelet was used to create a wavelet spectrum from these bed level measurements. Wavelet analysis is a tool to determine local variations of power within a time series to reconstruct bed forms. The dune profile was reconstructed from the wavelet spectrum by using representative dune length scales as a bandpass filter. The crests and troughs of the primary dunes were found by plotting the reconstructed dune profile on the smoothed bed profile (Savitzky-Golay filter). The celerity of the river dunes between two successive measurements was found by the cross-correlation technique. This method was used to determine the geometry and celerity of the dunes. The underwater volume of the ship is probably different per navigation direction since up sailing ships (left bank) are heavily loaded and down sailing ships (right bank) are less loaded. By analysing this bank effect, the results only showed significant differences of longer dune lengths at the outer sides of the river. Observations showed longer dune lengths at the right bank compared to the left bank. The passing distance from the bank and the underwater volume of the ship predominantly determine the effect of navigation on the groyne field hydrodynamics. Up sailing ships have, therefore, more impact on the hydrodynamics in the groyne field and cause scour holes that are larger and further located into the main channel at the left bank. Thus, the river shoals ('kribvlammen') in between the scour holes affect the dune length results at the outer sides of the river.

The ship movement was analysed with the AIS data. The MSSSI-number (ship's number) grouped the longitude and latitude of the ships. These data points were generalised per ship trajectory based on distance. These generalised ship trajectories together provided insights for the primary navigation tracks in the river. This method was used to determine the ship intensity in the river section. The groins affect the dune length in the navigation tracks. Observations also showed again a longer dune length in the left navigation track than in the right navigation track due to probably the cargo difference per navigation direction. Further work with CoVadem data (direct depth measurements underneath the ship) needs to be done to establish whether the dune height is really not affected by navigation. The ship intensity was also analysed between the low water periods since 17% more ships were observed in 2019 than in 2020. However, the significant differences in dune length and celerity are rather related to the difference in water level. For this difference in ship intensity, the effect of hydraulic conditions on the river dunes is, thus, stronger than the effect of ship movement.

This research concludes that no direct effect of navigation has been found on the geometry and celerity of the river dunes. Observations only showed an indirect effect of navigation on the river shoals which affected the dune length results due to the impact of navigation on the hydrodynamics in the groyne fields. This effect of navigation is related to the underwater volume of the ship, and not ship intensity. Future work needs to be carried out to quantify the effect of the underwater volume of the ship (related to under keel-clearance) on the geometry and celerity of river dunes by using the CoVadem data.

Contents

List of Figures and Tables	VI
<i>Figures.....</i>	<i>VI</i>
<i>Tables.....</i>	<i>VII</i>
List of symbols	VIII
1 Introduction	9
1.1 Context.....	9
1.2 Literature overview	11
1.3 Study objective.....	11
1.4 Outline	12
2 Background	13
2.1 Ship-induced water movement	13
2.2 Sediment transport processes.....	16
2.3 River dunes.....	18
3 Methodology.....	20
3.1 Conditions	20
3.1.1 Study area.....	20
3.1.2 Time series.....	20
3.2 River dunes.....	21
3.2.1 MBES data	21
3.2.2 River dune analysis	22
3.3 Navigation.....	25
3.3.1 AIS data.....	25
3.3.2 Ship intensity analysis.....	25
4 Results.....	27
4.1 River dune behaviour	27
4.2 Navigation.....	29
4.2.1 Bank effects	29
4.2.2 Ship intensity effects	32
5 Discussion	36
5.1 River dune behaviour	36
5.1.1 Dune length	36
5.1.2 Dune height	37
5.1.3 Dune celerity	38
5.1.4 Dune pattern	38
5.1.5 Summary.....	38
5.2 Navigation.....	39
5.2.1 Dune length	39
5.2.2 Dune height	42
5.2.3 Dune celerity	42
5.2.4 Navigation difference between the years	43
5.2.5 Practical applicability.....	43

6	Conclusions and recommendations	45
6.1	<i>Conclusions</i>	45
6.2	<i>Recommendations</i>	46
	References.....	47
	Appendices.....	52
A.	Sediment transport induced by navigation	53
B.	Script Jupyter Notebook ship intensity analysis	55
C.	Dune pattern Waal section Beneden-Leeuwen	56

List of Figures and Tables

Figures

Figure 1 and Figure 2: Maps of the average water depth at Erlecom and Nijmegen until 2014 (Rijkswaterstaat ON, 2018).....	10
Figure 3: Affected processes in the river by navigation. Used as literature overview. Adapted from (Earle, 2015; Jing.fm, 2021).....	13
Figure 4: Top view of the waves and currents around a ship (Verheij et al., 2008).	14
Figure 5: Top view of the waves and currents around a ship in practice.	14
Figure 6: Side view of the waves and current around a ship (Verheij et al., 2008).	15
Figure 7: Flow field behind the main propeller (Verheij et al., 2008).....	15
Figure 8: Shields curve (Shields, 1936).	17
Figure 9: Terms and parameters related to river dunes (Lokin, 2020).	18
Figure 10: Dune propagation based on the maximum sediment transport rate related to the dune crest. The green dot is the dune crest and the red dot is the location of the maximum sediment transport rate (Naqshband et al., 2017).....	19
Figure 11: Map of the area of interest in the Waal at Druten (Rivieren Nederland, 2021).....	20
Figure 12: Graph of the water level at Dodewaard for 2019 and 2020 (average bed level is 0.25 m – NAP).....	21
Figure 13: River bed based on MBES with a spatial resolution of 1x1 m at Druten in March 2019.	22
Figure 14: Graph of the line profile with the bed level over the length of the study area on 6 January 2020.....	23
Figure 15: Morlet wavelet with real part (solid) and imaginary part (dashed) (Lancia, 2014).	23
Figure 16: Wavelet spectrum for centreline of the Waal at Druten on 6 January 2020.....	24
Figure 17: Histogram of the speed difference per navigation direction for July 2020.	25
Figure 18: Map of AIS signals (red dots) within a single ship track (blue line) for the Waal.	26
Figure 19: Dune height (blue) and length (red) for the water level at the Waal section Dodewaard-Ochten for 2019-2020 (average bed level is 0.25 m – NAP).....	27
Figure 20: Dune celerity for the water level at the Waal section Dodewaard-Ochten for 2019-2020 (average bed level is 0.25 m – NAP).	28
Figure 21: Dune pattern of the crests during high water at the Waal section Druten for 17-03-2020 (water level of 8.92 m + NAP for a bed level of 0.25 m – NAP at Dodewaard). The rectangle in the bottom left of the Figure indicates Druten in the study area.....	29
Figure 22: Dune pattern of the crests during low water at the Waal section Druten for 07-08-2020 (water level of 3.98 m + NAP for a bed level of 0.25 m – NAP at Dodewaard). The rectangle in the bottom left of the Figure indicates Druten in the study area.....	29
Figure 23: Dune length over the river width for the water level at the Waal section Dodewaard-Ochten for 2019-2020 (average bed level is 0.25 m – NAP). The bottom half of the Waal’s width is the left bank and the top half is the right bank (seen from the discharge direction).	30
Figure 24: Dune height over the river width for the water level at the Waal section Dodewaard-Ochten for 2019-2020 (average bed level is 0.25 m – NAP). The bottom half of the Waal’s width is the left bank and the top half is the right bank (seen from the discharge direction).	30
Figure 25: Hexbin plot of the ship intensity at the Waal section Ochten for the low water period in 2019-2020. At the bottom right, a map has been added to show where Ochten is located within the study area.	32
Figure 26: Dune length and celerity for the water level at the Waal section Dodewaard-Ochten for the low water periods in 2019-2020 (average bed level is 0.25 m - NAP). The red colour indicates the navigation tracks and trendline from 2019 and the blue colour indicates the navigation tracks and trendline from 2020. The triangles correspond with the right navigation track and the circles with the left navigation track.....	34

Figure 27: Equilibrium dunes calculated in a steady current for different forcing's (Niemann et al., 2011)..... 37

Figure 28: Dune migration rate for the Waal discharge at Beneden-Leeuwen during the floods of 1995, 1997 and 1998 (Wilbers & Ten Brinke, 2003)..... 37

Figure 29: Dune migration rate for the discharge in the middle sand-bed section of the Waal during the flood of 1997 (Ten Brinke, Wilbers, et al., 1999)..... 37

Figure 30: Flow pattern in the groyne fields with a large and small distance between the groynes (Ten Brinke, Kruyt, et al., 1999). 39

Figure 31: The sediment transport volumes in kg/s for groyne fields with a large and small distance between the groynes (Ten Brinke, Kruyt, et al., 1999). 39

Figure 32: The interaction in flow between a ship and a characteristic groyne field along the Waal. The acceleration and deceleration of the flow (left) and the corresponding flow pattern (right) is visible during the passage of a ship (Ten Brinke et al., 2004). 41

Figure 33: Dune length over the river width for the water level at the Waal section Dodewaard-Ochten for 2019-2020 (average bed level is 0.25 m – NAP). The bottom half of the Waal's width is the left bank and the top half is the right bank (seen from the discharge direction). The dashed lines indicate the navigation tracks and the arrows indicate the navigation direction. 42

Tables

Table 1: Ship classification for the Waal river (Rijnvaartpolitierglement Art. 11.01, 1995; Verheij et al., 2008)..... 14

Table 2: Empirical river dune predictors..... 19

Table 3: Steps taken in ship intensity analysis to determine ship tracks..... 26

Table 4: The median dune length and height for the right and left bank in comparison to the overall river width for both low water periods in 2019 and 2020 (average bed level is 0.25 m – NAP). 31

Table 5: The median dune celerity for the right and left bank in comparison to the overall river width for both low water periods in 2019 and 2020 (average bed level is 0.25 m – NAP). 31

Table 6: The median dune length and height for the tracks with the most and least navigation for both low water periods in 2019 and 2020 (average bed level is 0.25 m – NAP)..... 33

Table 7: The median dune celerity for the tracks with the most and least navigation for both low water periods in 2019 and 2020 (average bed level is 0.25 m – NAP)..... 33

Table 8: Ship intensity for the low water period 2019-2020 (average bed level is 0.25 m – NAP). 34

Table 9: List of parameters for an average situation in the Waal between Nijmegen and Zaltbommel (italic parameters are determined below)..... 53

List of symbols

Symbol	Description	Unit
A_s	Underwater surface of the amidships cross-section	m^2
A_c	Underwater surface of the channel in the cross-section	m^2
B_s	Width of the ship	m
C	Chézy coefficient	$m^{1/2}/s$
C_{90}	Grain related Chézy coefficient	$m^{1/2}/s$
d	Diameter of the particle	mm
D	Sediment diameter	m
D_0	Diameter of the propeller	m
D_{50}	Average grain size diameter	m
D_{90}	90 th percentiles of the grain size distribution	m
D_*	Dimensionless particle parameter	-
g	Gravitational acceleration	m/s^2
h	Water depth	m
H	Dune height	m
i	Complex number	-
k_{sl}	Slope factor	-
k_t	Turbulence factor	-
L	Dune length	m
P	Rouse number / Power of the engine	- / W
R_p	Reynolds particles number	-
S_b	Bedload transport	kg/ms
T	Bedshear parameter	-
T_{nav}	Passage time ship	s
u_b	Velocity at the bed	m/s
u_*	Shear velocity	m/s
U	Velocity	m/s
U_r	Return current	m/s
V	Volume sediment	m^3
V_s	Sailing speed	m/s
w_s	Settling velocity	m/s
z_b	Vertical distance between propeller axis and the bed	m
Δ	Relative density	-
η	Non-dimensional time parameter	-
θ	Shields parameter	-
θ_{cr}	Critical Shields parameter	-
θ'	Particle mobility parameter	-
κ	von Kármán constant	-
ν	Kinematic viscosity	m^2/s
ρ_s	Density of sediment	kg/m^3
$\rho_{sed\ on\ bed}$	Specific mass of sediment on river bed	kg/m^3
ρ_w	Density of water	kg/m^3
τ_b	Bed shear stress	kg/ms^2
$\tau_{b\ cr}$	Critical bed shear stress	kg/ms^2
τ'_b	Bed shear stress related to grain roughness	kg/ms^2
ψ_0	Wavelet function	-
ω_0	Non-dimensional frequency	-
λ	Dune length	m
Δ	Dune height	m

1 Introduction

For integral river management, a program under the environmental law (in dutch: PoW¹) contains a policy framework to improve the river area in the Netherlands. This framework aims to design a future-proof river system e.g. navigation, nature and ecological water quality, freshwater availability and spatial economic developments (IRM team, 2021). The Rhine river in the Netherlands is essential for inland shipping. This river connects the main deep-sea ports of Rotterdam, Amsterdam and Antwerp, with the eastern hinterland, like the Ruhr area in Germany. However, the river bed erosion in combination with extremely dry periods causes challenges for river management because of the limited navigation depth for vessels.

Therefore, this chapter introduces these challenges as motivation to execute this research. The second paragraph summarises the corresponding literature. Chapter 2 gives a more extensive literature overview. The identified research gaps are based on the literature. These research gaps lead to the study objective with the corresponding research questions. The chapter ends with the outline of the thesis.

1.1 Context

Rijkswaterstaat contributes to the development of a future-proof river system for integral river management. However, effective river bed management proves to be difficult due to the non-uniform eroding river bed (fixed layers) and the decrease in water depth during droughts. As soon as these challenges are solved, the hypothesis is that river dunes become normative for the navigation depth in the river. However, the geometry and celerity of these river dunes may be affected by the water movement of navigation (Ten Brinke et al., 2004; Verheij et al., 2008; Wilbers & Ten Brinke, 2003). By quantifying this effect of navigation on river dunes, river bed management can be improved. These challenges are the drive for this research and are further explained below.

The river bed of the Waal is slowly being eroded over the past years. Based on Sieben (2009), the Waal eroded 3.0 cm/year in the upper section and 1.0 cm/year in the middle section during the period 1950-2000. Hendrikssen (2018) observed an erosion in the Waal of 1.5 cm/year in the upper section and 0.9 cm/year in the middle section during 2000-2015. An important cause of this river bed erosion is the increase of flow rate by the removal of bends and the addition of groynes during the 18th and 19th century (Ylla Arbós et al., 2020). The extraction of sand and gravel in Germany also reduces the sediment supply (Wolters et al., 2020)². Changes in the bed level also affects other river functions, for example nature and ecological water quality (IRM team, 2021).

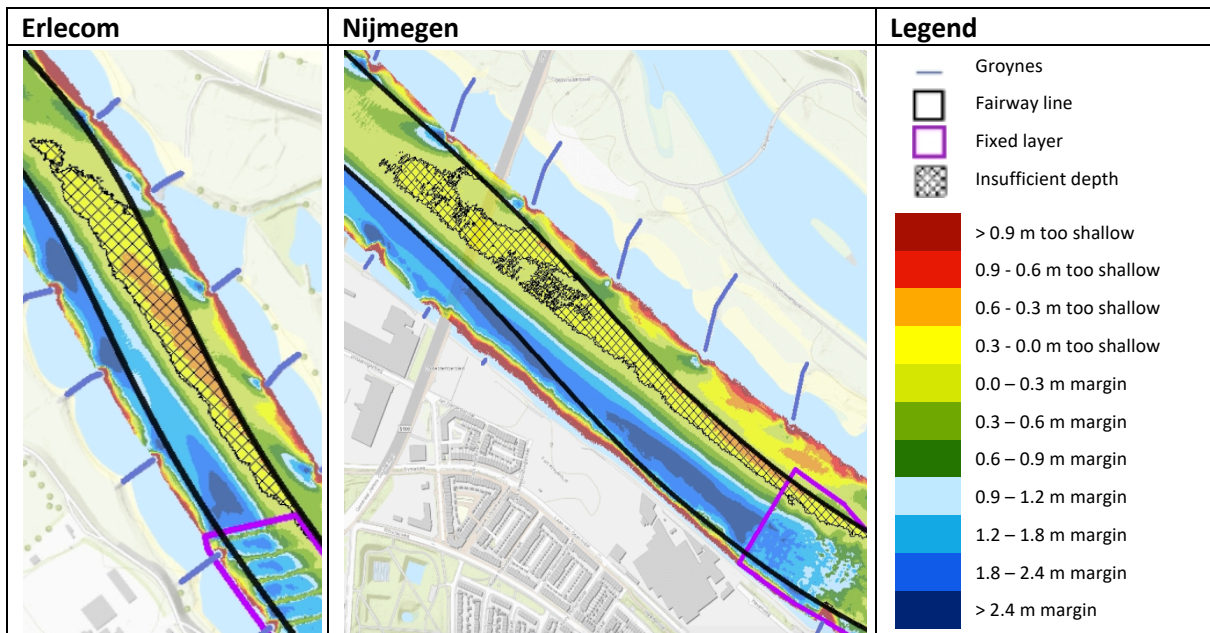
However, the river bed is not eroding uniformly based on measurements. Hulhuizen, Erlecom, Nijmegen, Ophemert and St. Andries are the locations with the lowest water depth in the Waal (in Dutch: MGD³). By observing the measurements, the bed level increases in the inner bends because of spiral flow. This spiral flow causes sedimentation downstream of fixed layers on the inside of the bend (Sloff and Mosselman, personal communication, April 2, 2021). These locations cause limited navigation depth, which can be seen for example in Figure 1 at Erlecom (Rijkswaterstaat ON, 2018). These sedimentation spots cannot be dredged otherwise cables and pipes are exposed. Fixed layers do not erode along with the river due to the heavy bed material (Wolters et al., 2020)². Not only the sedimentation downstream of the fixed layer is critical, the navigation depth is also limited at the fixed layer of Nijmegen. This can be seen in Figure 2 (Rijkswaterstaat ON, 2018). Besides fixed layers, and cables and pipes, hydraulic structures do also not erode along with the river. The guideline of 40% keel clearance in the river is causing challenges for river bed management at the five mentioned locations with the least water depth (Wolters et al., 2020)².

¹ Programma onder de Omgevingswet (in Dutch)

² Source from Rijkswaterstaat (no public access)

³ Minst Gepeilde Dieptes (in Dutch)

Figure 1 and Figure 2: Maps of the average water depth at Erlecom and Nijmegen until 2014 (Rijkswaterstaat ON, 2018).



During dry periods, the decreased water depth hampers inland navigation (Wolters et al., 2020)⁴. This leads to different reactions and effects. Low water forces vessels to transport a significantly lower maximum load, to make sure they have enough keel clearance (Steel, 2020). A low water depth of approximately 1.7 m was measured in the Rhine branches on 22 October 2018 (Wolters et al., 2020)⁴. This resulted in losses in the German economy and the Dutch construction sector because of less supply of goods in 2003 and 2018 (Jonkeren et al., 2008; Martin & Boerop, 2019). The estimated low water effect on the German industrial production was almost 5 billion euros in 2018 (Wolters et al., 2020)⁴. The prediction is that the frequency, duration and extremity of dry periods will increase even further in the future (Copernicus, 2020). Therefore, droughts cause limited navigation depth in the river.

If sufficient water depth is created at the five locations with the least water depth, the hypothesis is that river dunes become normative in the Waal. Wilbers & Ten Brinke (2003) measured the bed at three sections in the Dutch Rhine. These measurements were executed during a flood wave: at the start of the flood; at the peak of the flood; at the maximum dune height; and the end of the flood. The dominant bed form is river dunes in the sandy reaches of the river system, which is especially the case in the Waal. River dunes grow and decay during floods. Thus, flow conditions affect the geometry and propagation of river dunes (Julien et al., 2002; Wilbers & Ten Brinke, 2003).

Navigation affects the flow conditions in the river by waves, currents and turbulence (Verheij et al., 2008). Inland navigation plays an important role in river management since a daily average of 600 ships passes the border between the Netherlands and Germany (CCR, 2021). Changes in flow conditions alter the sediment transport in a river. Especially return currents and turbulent propeller jets, induced by navigation, affect the sediment transport (Lenselink, 2011; Schiereck, 1993). Changes in sediment transport alter the river bed. However, to what extent navigation influences sediment transport and the river bed is not known. Determining the effect of navigation on river dunes could help to resolve the limited navigation depth. Therefore, knowledge needs to be gained on the quantification of the effect of inland navigation on the geometry and celerity of river dunes to improve river bed management.

⁴ Source from Rijkswaterstaat (no public access)

1.2 Literature overview

The Rhine and the Waal rivers are essential inland waterways within the Netherlands. The most common ship types in these inland waterways are the motor ships and the push tow convoys. The Dutch Rhine and the Waal are classified as VIc waterways according to PIANC⁵. This classification almost corresponds with the largest navigation types (Verheij et al., 2008).

The water movement induced by navigation can be separated into three hydraulic characteristics: primary waves, secondary waves and propeller jets. The return current forces the primary waves. Water pushed around and underneath the ship in the opposite direction of the movement of the ship causes the return current (Verheij et al., 2008). The maximum return current can be measured underneath the ship because of the decrease in under keel clearance (Dorst et al., 2016). Wave heights from 0.2 to 0.5 meters characterize the primary waves (Schiereck, 1993). Secondary waves are not taken into account in this research due to their minimal effect on the river bed (Lenselink, 2011). Propeller jets are locally increased velocities in the river by the propulsion systems. The most important propulsion systems are the main propellers, the bow thrusters and stern thrusters (Verheij et al., 2008). Thus, navigation alters the currents in the river.

The interplay between sediment characteristics and flow conditions determines whether or not sediment gets into motion. If the shear stress is higher than the resistance of the sediment (Shields parameter > critical Shields parameter), sediment gets into motion (Shields, 1936a; van Rijn, 1993). The equation of Van Rijn is the most suitable to predict sediment transport induced by navigation due to the accurate performance for high velocities ($\bar{u} > 1\text{m/s}$).

The sand bed in the Waal river is characterised by river dunes (Julien et al., 2002; Wilbers & Ten Brinke, 2003). The horizontal distance between two successive bedform troughs indicates the dune length. The vertical distance between the crest and the following trough defines the dune crest. The largest river dunes are the primary dunes. Secondary dunes are superimposed dunes on the primary dunes. The dune decays if the location of the maximum sediment transport rate is downstream of the dune crest, the dune grows if this location is upstream of the dune crest and the dune maintains if this location is equal to the dune crest. The response of the dune shape could lag with the change in flow conditions, which is called hysteresis. As a result, the dune shape in practice may deviate from the expected results. Empirical dune predictors can estimate the length and height of the river dunes. The following empirical relations can be used to determine the length and height of the dunes: Shinohara & Tsubaki (1959), Allen (1968), Van Rijn (1984c), Bradley & Venditti (2017) and Wilbers (2003).

1.3 Study objective

Based on the literature, it is known that navigation induces water movement by return currents and turbulent propeller jets (Lenselink, 2011; Schiereck, 1993; Verheij et al., 2008). This water movement increases the flow and the sediment transport in the river (van Rijn, 1993). An increase in sediment transport affects the dimensions and the propagation of river dunes (Naqshband et al., 2017). Currently, it is thus known that navigation affects sediment transport and river dunes. However, to what extent navigation affects sediment transport and river dunes is not determined. Based on the literature review, two knowledge gaps are discovered. These knowledge gaps are given below:

Knowledge gap 1: Up sailing ships towards the Ruhr area are heavily loaded and down sailing ships towards the Port of Rotterdam are significantly less loaded in the Waal (Ten Brinke et al., 2004; Wilbers & Ten Brinke, 2003). The difference in cargo between those two directions results in different waves, currents and turbulence induced by ships (Dorst et al., 2016; Lenselink, 2011; Schiereck, 1993; Verheij et al., 2008). Ten Brinke et al. (2004) showed results of more erosion at the right bank than at the left bank due to heavier loaded vessels and barges. However, current research is only focused on flume experiments instead of river bed measurements.

⁵ Permanent International Association of Navigation Congresses

Knowledge gap 2: Studies on the effect of ship movement on the river bed mainly focus on the passage of a single vessel. The empirical relations to determine the effect on the river bed are also mostly based on flume experiments (CIRIA, 2007; Lenselink, 2011; Schiereck, 1993; Verheij et al., 2008). Flume experiments differ from field measurements due to variable conditions in rivers. No study is also available with accurate ship position data from the river as obtained by AIS.

The knowledge gaps result in the study objective and research questions. The objective of this thesis is achieved by answering the research questions. The study objective and research questions are given below. The numbering of the knowledge gaps corresponds with the numbering of the research questions.

To quantify the effect of inland navigation on the geometry and celerity of river dunes to improve river bed management.

Research question 1: What are the differences in river dune geometry and celerity for the right and the left bank for a straight river section based on the MBES of the Waal?

Research question 2: How is the geometry and celerity of river dunes affected by ship movement intensity based on the ship-position data from the AIS of the Waal?

1.4 Outline

Chapter 2 describes the background literature for this research. Chapter 3 explains the research methodology. This chapter describes the used method for the identification of the river dunes and the ship intensity. Chapter 4 provides the results that are obtained in this study. This chapter starts by describing the general behaviour of the river dunes. Thereafter, results are presented to determine the effect of navigation. Chapter 5 discusses the obtained results. First, the chapter validates the general behaviour of the river dunes. The next section discusses the effect of navigation on the geometry and celerity of river dunes. The last chapter, chapter 6, outlines the main conclusions and limitations of this research. Also, recommendations are given for future research.

2 Background

The background is an extension of the literature overview given in the previous chapter (paragraph 1.2). This chapter is separated into three topics. As already discussed, navigation affects the flow conditions in the river by waves and currents. This chapter starts by discussing this water movement induced by navigation (processes 1 and 2 in Figure 3). The interplay between the flow conditions and the sediment characteristics determines if sediment transport takes place. The second paragraph explains this interplay since variations in the flow conditions alter the sediment transport in the river (process 3 in Figure 3). The alteration of flow conditions and sediment transport affect the river dunes. The third paragraph, therefore, discusses the geometry and propagation of river dunes (process 4 in Figure 3). Figure 3 summarises the literature that will be discussed in this chapter.

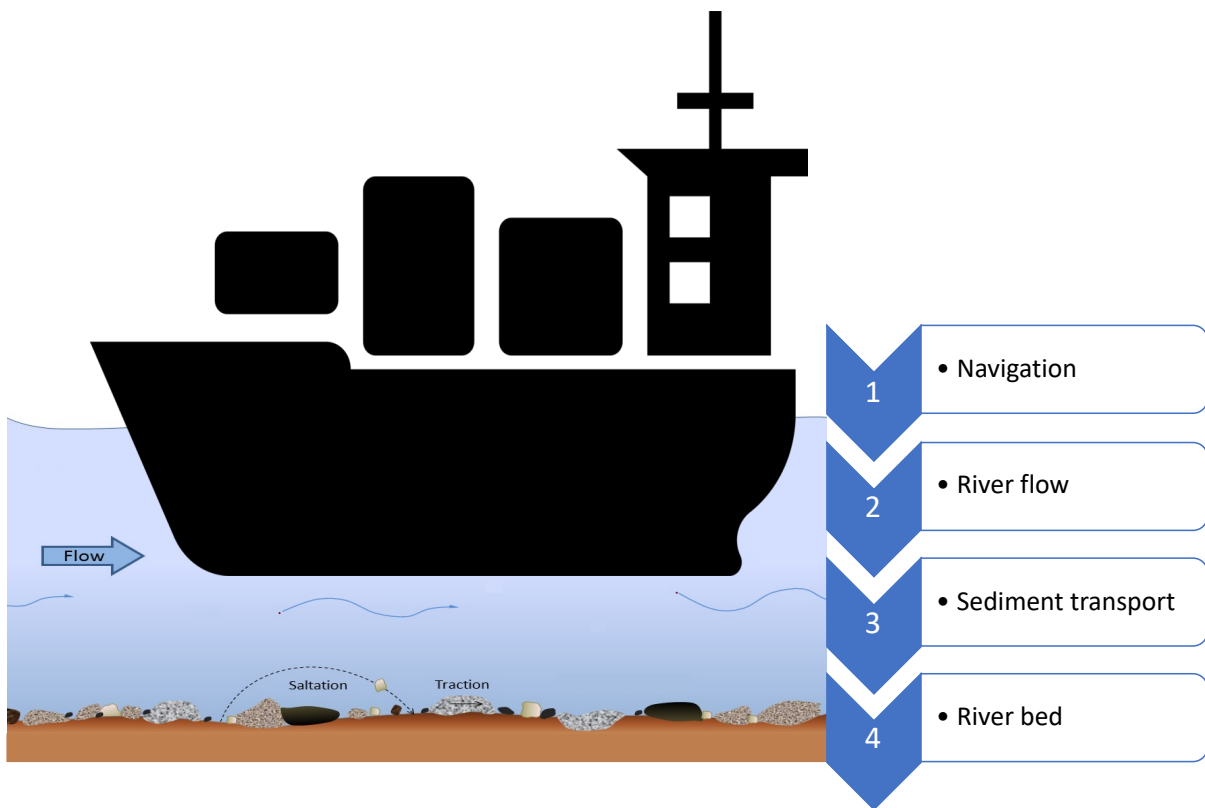


Figure 3: Affected processes in the river by navigation. Used as literature overview. Adapted from (Earle, 2015; Jing.fm, 2021).

2.1 Ship-induced water movement

Inland navigation transfers cargo. Motor vessels are the most common ship type on the inland waterways. In total, 7033 motor vessels were observed in the Rhine for 2019 (CCNR, 2020). Examples of motor vessels are general cargo vessels, bulk vessels, container vessels, roro (roll-on and roll-off) vessels, car carriers, tanker vessels and cruise vessels. Push tow convoys are also a ship type on the inland waterways, but less common than most of the examples above. Only 1319 push tow convoys were counted in the Rhine for 2019 (CCNR, 2020). Push tow convoys consist of a push boat connected with barges, to manoeuvre as one vessel (Verheij et al., 2008). The classification of PIANC by Rijkswaterstaat classifies the Waal river as essential waterway (Vic) (UNECE, 2012). Table 1 shows the maximum permissible dimensions per ship type for the Waal river.

Table 1: Ship classification for the Waal river (Rijnvaartpolitiereglement Art. 11.01, 1995; Verheij et al., 2008).

Ship type	Designation	Length (m)	Beam (m)	Draught (m)	Tonnage (T)
Motor vessels & barges		135	22.80	-	-
Pushed conveyors	6 barges, 2 wide & 3 long	270-280	22.80	2.50-4.50	9,600-18,000
	6 barges, 3 wide & 2 long	193-200	33.00-34.20	2.50-4.50	9,600-18,000

Navigation induces water movement by waves, currents and turbulence. The hypothesis is that up sailing ships towards the Ruhr area are heavily loaded and down sailing ships towards the Port of Rotterdam are significantly less loaded in the Waal (Ten Brinke et al., 2004; Wilbers & Ten Brinke, 2003). Vessels that are sailing upstream have the right to choose the optimal side of the waterway. Newer and bigger vessels often choose the deepest side of the waterway to use the power of the engine, while other vessels normally choose the shortest route with inside bends (Vrijaldenhoven, personal communication, March 15, 2021). Usually, up sailing ship follow the left bank and down sailing ship follow the right bank (Wilbers & Ten Brinke, 2003). The draft of the vessel, related to the cargo quantity, determines the strength of the waves, currents and turbulence induced by navigation. Wilbers and Ten Brinke (2003) and Ten Brinke et al. (2004) argue that the difference in ship movement may cause differences in the bed between the banks.

Three hydraulic characteristics distinguish the water movement induced by a ship: primary waves, secondary waves and propeller jets (Verheij et al., 2008). All the waves and currents can be seen in Figure 4 and in practice in Figure 5. The return current (related to the primary waves) and the propeller jets, induced by navigation, primarily cause bed erosion and, therefore, secondary waves are not considered any further (Lenselink, 2011).

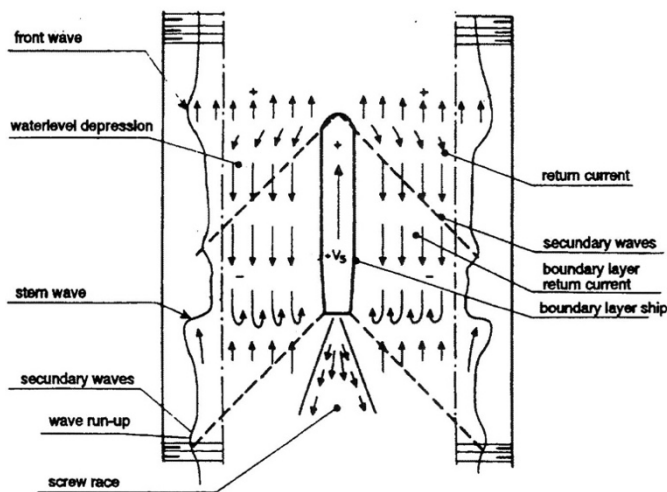


Figure 4: Top view of the waves and currents around a ship (Verheij et al., 2008).



Figure 5: Top view of the waves and currents around a ship in practice.

Primary waves

The height of the primary waves varies between 0.2-0.5 meters in rivers. The water depth, vessel draft and keel-clearance strongly relate to the height of the primary dunes (Schierreck, 1993). The return flow and a follow flow create this water movement. Water flowing around and underneath the ship forms the return current. The return current is directed in the opposite of the movement of the ship. This water movement also changes the water level around a ship, see Figure 6 (Verheij et al., 2008). It causes a front wave (in front of the ship), a stern wave (behind the ship) and in between a water level drawdown. Water flows from the bow wave (return flow) and stern wave (follow flow) to the water level depression (Ten Brinke et al., 2004). This decrease in water level pulls the ship down towards the river bed, which is called squat (Verheij et al., 2008).

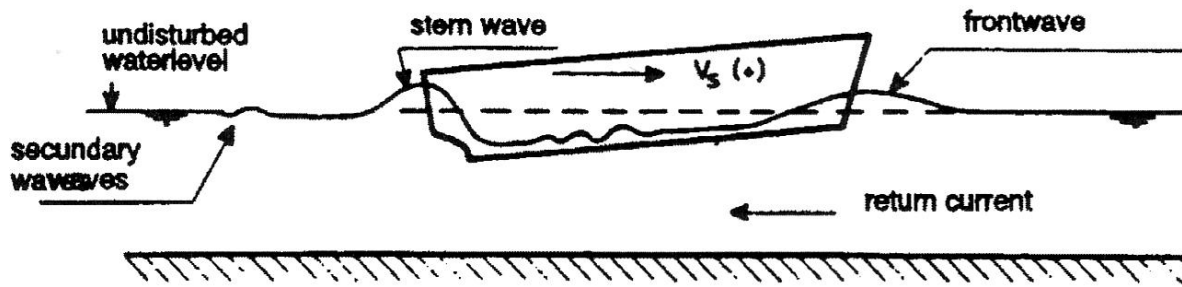


Figure 6: Side view of the waves and current around a ship (Verheij et al., 2008).

By combining the Bernoulli equation with the continuity equation, the return current velocity can be determined. This can be used as input for the sediment transport formulation. The following parameters need to be known to solve equation 1 for the return current velocity (U_r): the speed of the ship, the water depth, the underwater surface of the amidships cross-section and the underwater surface of the channel in the cross-section (Verheij et al., 2008).

$$\frac{(V_s + U_r)^2 - V_s^2}{2gh} - \frac{U_r}{V_s + U_r} + \frac{A_s}{A_c} = 0 \quad (1)$$

V_s = speed of the ship compared to the bank [m/s]

U_r = average return current velocity compared to the bank [m/s]

g = gravitational acceleration [m/s²]

h = water depth [m]

A_s = underwater surface of the amidships cross-section [m²]

A_c = underwater surface of the channel in the cross-section [m²]

Propeller jets

The flow of the propulsion systems also causes water movement. The propeller of a ship increases the velocity in the river locally. This flow, induced by a ship's propeller, can be seen as a turbulent jet due to the higher velocity compared to the surrounding. Figure 7 shows the flow field behind the main propeller (Verheij et al., 2008).

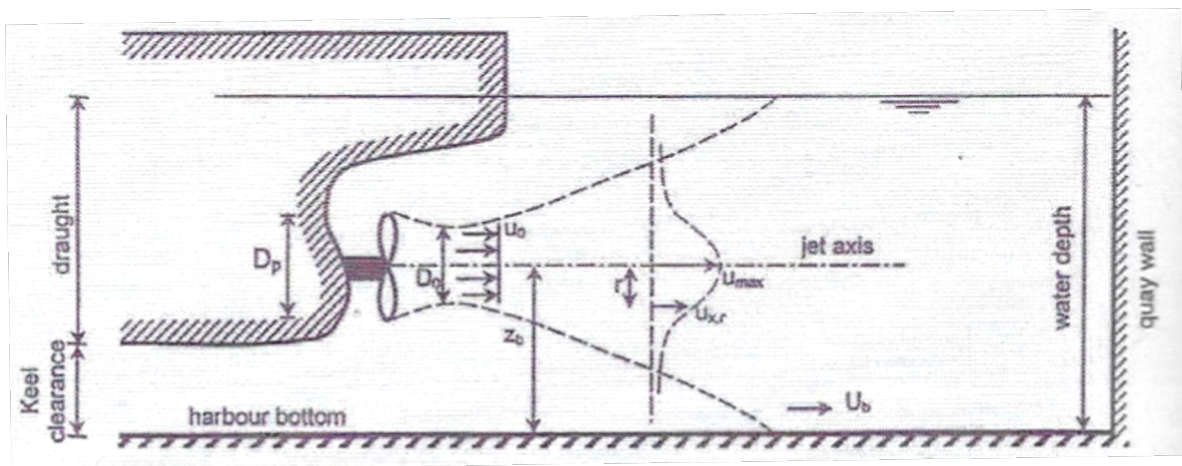


Figure 7: Flow field behind the main propeller (Verheij et al., 2008).

Besides the main propellers, bow and stern thrusters also induce turbulent jets and all three together are the most important propulsion systems. These thrusters are directed perpendicular to the axis of the ship. The function of these thrusters is to allow the ship to manoeuvre independently (Verheij et al., 2008).

The turbulent jets from the propulsion systems can result in bed erosion, especially if the ship lies still or is manoeuvring. The velocity at the bed can be determined based on equation 2. However, this equation is overestimating the velocity at the bed if the ship is already sailing. Therefore, the velocity at the bed should be decreased with half the speed of the ship in case of an already sailing vessel (Schiereck, 1993).

$$u_b = 0.3u_0 \frac{D_0}{z_b} \quad (2)$$

u_b = velocity at the bed [m/s]

u_0 = outflow velocity [m/s] = $1.15 \left(\frac{P}{\rho_w D_0^2} \right)^{0.33}$

P = power of the engine [W]

ρ_w = density of water [kg/m³]

D_0 = diameter of the propeller [m] ≈ 0.7 * ship's draught

z_b = vertical distance between propeller axis and the bed [m]

The stability of the bed for turbulent propeller jets can be determined by equation 3. The turbulence coefficient should be 5.2 (k_t^2). This turbulence factor should be increased to the value 6 (k_t^2) for the maximum effect of the turbulent propeller jet on the bed. The stability of the bed can also be checked for the return current velocity by replacing the velocity at the bed (u_b) with the return current (U_r), see equation 1 (CIRIA, 2007).

$$\frac{u_b^2/2g}{\Delta D_{50}} = 2 \frac{k_{sl}}{k_t^2} \quad (3)$$

Δ = relative grain density [-]

D_{50} = median grain size [m]

k_{sl} = slope factor [-]

k_t = turbulence factor [-]

2.2 Sediment transport processes

The interplay between the flow conditions and the sediment characteristics determines if sediment can move in the river. The particle characteristics (e.g. shape and density) and the bulk characteristics (e.g. cohesion and friction angle) determine together the sediment characteristics. Shear stress is the force of the water on the particles of the river bed. If the shear stress is above a certain threshold, the sediment starts to move. The shear stress is incorporated in the determination of the grain mobility parameter, also called the Shields parameter (θ). Van Rijn (1993) composed equation 4 to determine the Shields parameter.

$$\theta = \frac{\tau_b}{(\rho_s - \rho)gD} \quad (4)$$

θ = Shields parameter [-]

τ_b = bed shear stress [kg/ms²]

ρ_s = density of sediment [kg/m³]

D = sediment diameter [m]

The critical Shields parameter is the resistance to sediment transport. If the Shield parameter is larger than the critical Shields parameter, the sediment gets into motion. The critical Shields parameter can be found by the Shields curve, given in Figure 8 (Shields, 1936b). Brownlie (1981) presented a smooth fit for the Shields curve based on the Reynolds particle number, see equations 5 and 6.

$$R_p = \frac{D\sqrt{\Delta g D}}{\nu} \quad (5)$$

R_p = Reynolds particles number [-]

ν = kinematic viscosity [m²/s]

$$\theta_{cr} = 0.22R_p^{-0.6} + 0.06 \exp(-17.77R_p^{-0.6}) \quad (6)$$

θ_{cr} = critical Shields parameter [-]

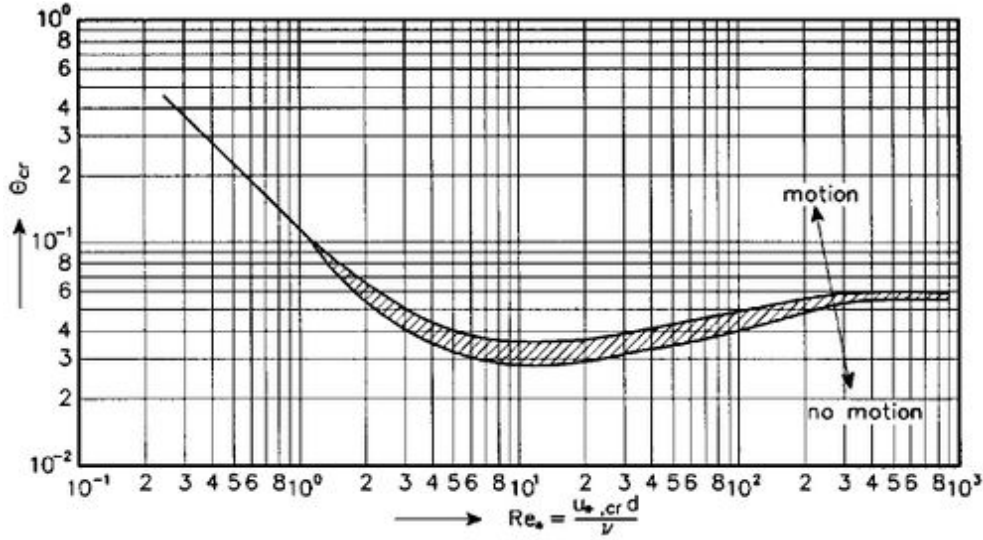


Figure 8: Shields curve (Shields, 1936).

The following forces act on a particle on the bed: buoyancy (F_L), gravity (F_G), drag (F_D) and resistance (F_L). The following forces act on the particle if the sediment moves: buoyancy, gravity, drag and turbulence. If the upward force, buoyancy, is higher than the downward force, gravity, the particle keeps on moving. The settling velocity follows from the Stokes' law and is applicable to sediment particles in suspension. By the addition of turbulence, the settling velocity depends on the size of the particle. Van Rijn (1993) transformed the settling velocity equation into three equations based on the diameter of the particle (Ferguson & Church, 2004):

$$0.01 < d \leq 0.1 \text{ mm} \quad w_s = \frac{\Delta g d^2}{18\nu} \quad (7)$$

$$0.1 < d \leq 1.0 \text{ mm} \quad w_s = \frac{10\nu}{d} \left(\sqrt{1 + \frac{0.01\Delta d^3}{\nu^2}} - 1 \right) \quad (8)$$

$$1 \text{ mm} < d \quad w_s = 1.1\sqrt{\Delta g d} \quad (9)$$

w_s = settling velocity [m/s]

d = diameter of the particle [mm]

The van Rijn sediment transport equation gives the most accurate predictions in rivers (Abdel-Fattah et al., 2004; Bisantino et al., 2010; van den Berg & van Gelder, 1993; Voogt et al., 1991). For sediment transport induced by navigation as sudden flux is the Van Rijn equation also the most suitable due to the accurate predictions for high velocities ($\bar{u} > 1\text{m/s}$) (van den Berg & van Gelder, 1993).

Navigation temporarily increases sediment transport in the river. The calculation can be found in Appendix A: Sediment transport induced by navigation. For an average situation in the Waal between Nijmegen and Zaltbommel, a push barge combination sailing at 2.56 m/s causes a return current of 0.39 m/s. This situation causes an effective shear stress of 38.65 kg/ms^2 , which corresponds to bed load transport according to the Rouse number ($P > 2.5$). By using the bed load transport rate of Van Rijn (1984a), the push barge combination induces a bed load transport of $1.42 \cdot 10^{-4} \text{ kg/ms}$. This results in $1.81 \cdot 10^{-4} \text{ m}^3$ during a passage duration of 60 seconds for the ship. A situation without a ship, so natural flow, only causes a transport of $2.13 \cdot 10^{-5} \text{ m}^3$ bed load in the same time. A single ship passage causes, thus, a bed load transport increase, almost ten times greater than during natural flow.

2.3 River dunes

The stoss slope (upstream) is gentle in comparison to the lee slope (downstream) for river dunes. On the exact meaning of the terms dune length and dune height is no consensus. In this study, the horizontal distance between two successive bedform troughs defines the dune length. The vertical distance between the crest and the following trough is the dune height (van der Mark et al., 2008). Figure 9 shows the terms and parameters related to river dunes.

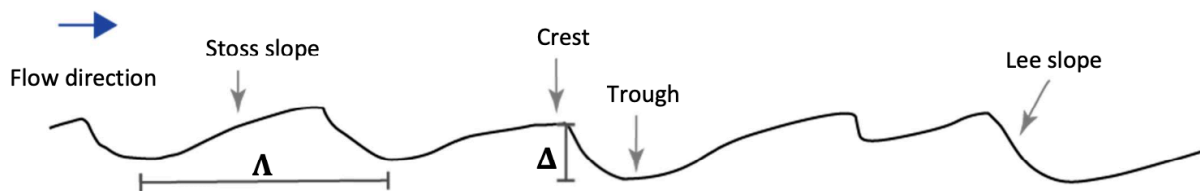


Figure 9: Terms and parameters related to river dunes (Lokin, 2020).

The largest river dunes are the primary dunes. Secondary dunes are shorter and smaller and form on the primary dunes during the falling period of the flood wave (Julien et al., 2002). These secondary dunes form during the decrease in discharge of the flood wave because the sediment transport is not sufficient anymore to decrease the primary dunes in length. Therefore, the smaller secondary dunes form on the primary dunes (Paarlberg et al., 2010). Ranges for the height and length of the dunes are given in the river dune analysis in section 3.2.2. Assumed is that bed load transport determines the formation of river dunes (van Rijn, 1984a).

The location of the maximum sediment transport rate in comparison to the dune crest determines the propagation of river dunes. Figure 10 indicates three situations that result in dune conservation (situation 1), dune growth (situation 2) or dune decay (situation 3). The initial bed perturbation is assumed to be stable, so spatial lag is not considered. The first situation indicates dune maintenance because the location of the maximum sediment transport is equal to the position of the dune crest. The flow deposits sediment on the stoss slope and the dune crest if the location of the maximum sediment transport rate is upstream of the dune crest. This results in the second situation, which indicates dune growth. Dune decay occurs in the third situation when the location of the maximum sediment transport lies downstream of the dune crest. The deposition of sediment at the lee slope and dune crest is not sufficient compared to the eroded sediment at the stoss slope and dune crest (Naqshband et al., 2017). Thus, the dune shape can be determined based on the location of the maximum sediment transport rate.

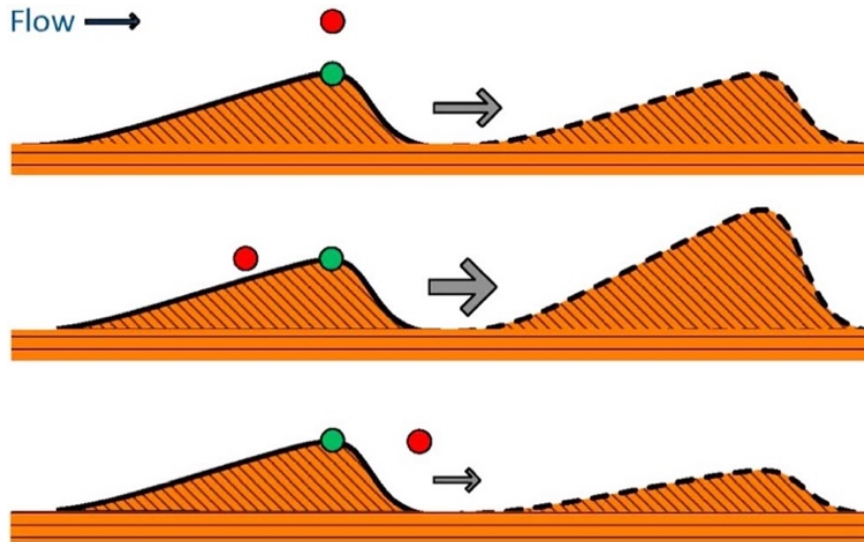


Figure 10: Dune propagation based on the maximum sediment transport rate related to the dune crest. The green dot is the dune crest and the red dot is the location of the maximum sediment transport rate (Naqshband et al., 2017).

Empirical dune prediction models can be used to estimate the length and the height of river dunes. Dunes are exposed to variable flow conditions in rivers. Therefore, the empirical relations of Shinohara & Tsubaki (1959), Allen (1968), Van Rijn (1984c), Bradley & Venditti (2017) and Wilbers (2003) can be used, within their specific validity domain. All of these predictors are based on field data. Table 2 shows the dune predictors.

Table 2: Empirical river dune predictors.

River dune height	River dune length	Source
$H = 2.1 * h(\theta')^{1.2}$	$L = 4.2 * h$	(Shinohara & Tsubaki, 1959)
$H = 0.086 * h^{1.19}$	$L = 1.16 * h^{1.55}$	(Allen, 1968)
$H = 0.11h \left(\frac{D_{50}}{h}\right)^{0.3} (1 - e^{-0.5T})(25 - T)$	$L = 7.3 * h$	(van Rijn, 1984c)
$H = \frac{h}{7.7}$	$L = 5.9 * h$	(Bradley & Venditti, 2017)
$H(t) = H_{(t-1)} + (1 - e^{-0.12\Delta t})(H_{\infty,t} - H_{(t-1)})$ $H_{\infty,t} = 0.086 * h^{1.19}$ if $\tau_b < 7$ $H_{\infty,t} = 0.11h \left(\frac{D_{50}}{h}\right)^{0.3} (1 - e^{-0.5T})(25 - T)$ if $\tau_b > 7$		(Wilbers, 2003)

3 Methodology

The methodology of this research describes the steps that were taken to come to the necessary results. The first step in the process was to define the river section and time interval as conditions for the data analysis. For the data analysis, the methodology is divided into two sections: river dunes and navigation. The river bed was analysed in order to identify the river dunes by using the MultiBeam Echo Sounding (MBES) for the Waal. The wavelet analysis accurately determined the geometry and celerity of the river dunes. The section about navigation describes the method to obtain the ship movement in the Waal. The Automatic Identity System (AIS) collected signals of the position of all the ships. The ship track was extracted from these signals by interpolation. This method was used in order to gain insights into the river dunes for periods of different ship intensity, but approximately equal discharges.

3.1 Conditions

This paragraph describes the domain for the data analysis. The study area was assessed by selecting an appropriate river stretch in the Waal using inclusion criteria. The time period was chosen by selecting the right water conditions. The nearest water measurement station to the study area was used to obtain the water conditions. The chosen study area and the period of time were used as conditions for the data analysis.

3.1.1 Study area

The most suitable stretch in the Waal is the river section at Druten (see Figure 11). The following criteria were used to select a proper area: a minimal effect of river interventions, no tidal influence and a straight river section. The effect of river interventions on the area of study needed to be reduced, to focus specifically on the effect of navigation on the river bed. Fortunately, no fixed layer (Erlecom, Nijmegen and St. Andries) or longitudinal dam (Tiel) is located near Druten. The tide is normally observable up to Zaltbommel and at very low discharge ($< 900 \text{ m}^3/\text{s}$) up to Tiel in the Waal (Reeze et al., 2017). Zaltbommel and Tiel are respectively 35 and 15 kilometres downstream⁶ from Druten. Druten, therefore, has no tidal influence. A straight river section was chosen to decrease the effect of bend processes. Groynes are within this river section roughly 200 meters apart.



Figure 11: Map of the area of interest in the Waal at Druten (Rivieren Nederland, 2021).

3.1.2 Time series

Navigation has the largest effect on the river bed during a period of small water depth as the keel-clearance is then decreased. A decrease in keel-clearance results in an increase of the return current velocity (see equation 1). The propeller velocity on the river bed also increases due to the decrease in vertical distance between the propeller axis and the bed (see equation 2). The effect of navigation increases, thus, on the river dunes if the water depth decreases. This is also shown by Dorst et al (2016) and Ten Brinke et al. (2004). At Lobtj, the average discharge is $2225 \text{ m}^3/\text{s}$ is equal to a water level of $9.40 \text{ m} + \text{NAP}$ (Reeze et al., 2017). The closest measurement location for the water level to the area of interest is at Dodewaard. The average water level at Lobtj corresponds with a water level of $5.90 \text{ m} + \text{NAP}$ at Dodewaard (Rijkswaterstaat, 2018). The average bed level is $0.25 \text{ m} - \text{NAP}$ at Dodewaard.

⁶ The tide enters the Waal from the sea, thus in opposite direction of the river discharge

This research only focused on periods with water levels that are lower than the average water level at Dodewaard ($< 5.90 \text{ m} + \text{NAP}$).

The availability of data sets was also taken into account by selecting the time period. The AIS data for the second half-year of 2018 was not available at Rijkswaterstaat. The year 2018 was, therefore, not considered since the required low water period occurred within this not available half-year. Suitable time periods were 'similar' low water periods over two different years to compare the periods on ship intensity. Seasonal effects were excluded by choosing the same months for the years with similar water levels. This is needed to gain insights into the effect of ship movement on river dunes over years (related to RQ2).

The months April, July, August and September had a similar low water level in 2019 and 2020. However, observations showed before April a much longer period of high water in 2020, than in 2019. The geometry of the river dunes was clearly different for both years at the start of April. The month April of 2019 and 2020 was, therefore, excluded in this research. The months July, August and September were suitable for 2019 and 2020 since the water level was constantly lower than $5.90 \text{ m} + \text{NAP}$ and the river conditions before July were quite similar. Figure 12 shows a graph of the water level at Dodewaard for 2019 and 2020. The average bed level for the entire study area is $0.25 \text{ m} - \text{NAP}$. The blue line shows the water level for 2019 and the orange line shows the water level for 2020. The red line is the average water level of $5.90 \text{ m} + \text{NAP}$ at Dodewaard. The grey area indicates the suitable low water period.

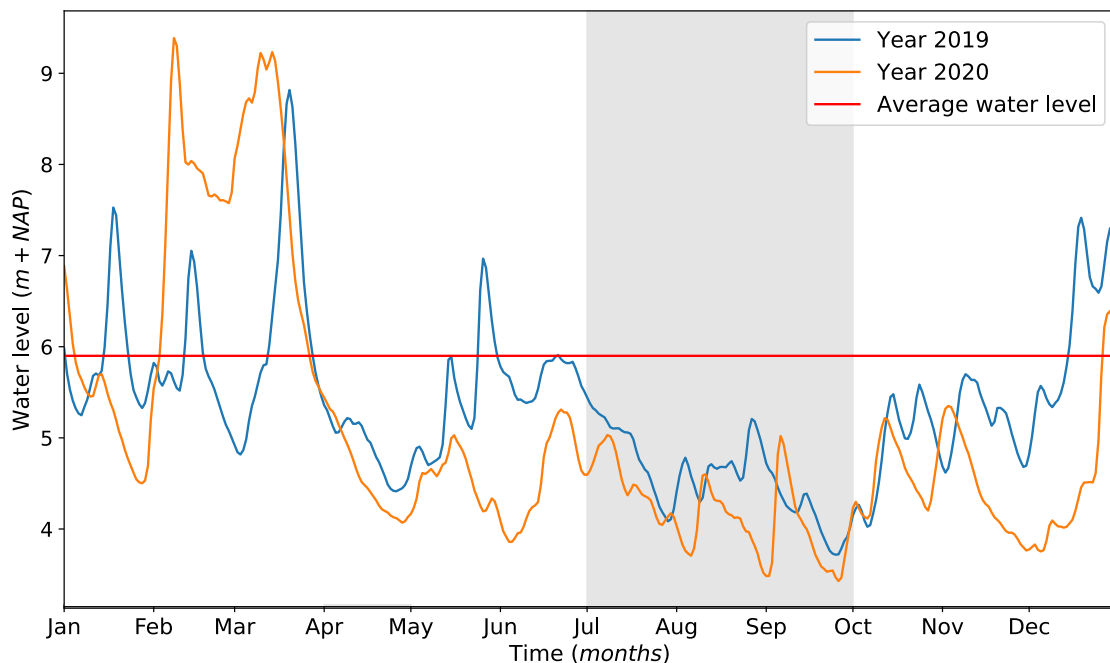


Figure 12: Graph of the water level at Dodewaard for 2019 and 2020 (average bed level is $0.25 \text{ m} - \text{NAP}$).

3.2 River dunes

The MBES data provided bed level measurements of the Waal. Many different bed forms were visible in the river bed. The wavelet analysis was used to create a wavelet spectrum to identify the river dunes in the bed level profile. The river dunes were analysed on the geometry and the celerity. The celerity of the river dunes was found by the cross-correlation technique.

3.2.1 MBES data

Data of the river bed was collected by MBES for Rijkswaterstaat. MBES is an acoustic technique based on a sound reflection on the river bed. This sound reflection is translated into a height with respect to Amsterdam Ordnance Datum (NAP) (de Ruijsscher et al., 2020). The data set contained, thus, bed

measurements of the Waal, which covered the full riverbed on a 2D grid (see Figure 13). The grid had a spatial resolution of 1x1 m. The MBES measurements were executed almost once per two weeks. Therefore, the temporal resolution of this data set was roughly two weeks.

The measurements carried out on 02-08-2019 and 12-11-2020 were disregarded since a large part of the study area contained unrealistic bed level values. By converting this data into NaN values, the determined dune length and height clearly deviate from the rest. Both measurements were, therefore, excluded.

The measurements were carried out for Rijkswaterstaat to monitor and manage the riverbed. This allows Rijkswaterstaat to take measures at the right time for example against non-uniform erosion. The dredging strategy is, therefore, determined based on these measurements to prevent danger for navigation. The information is also used to understand the river bed dynamics to improve river bed management in the future. The data set was used for all research questions.

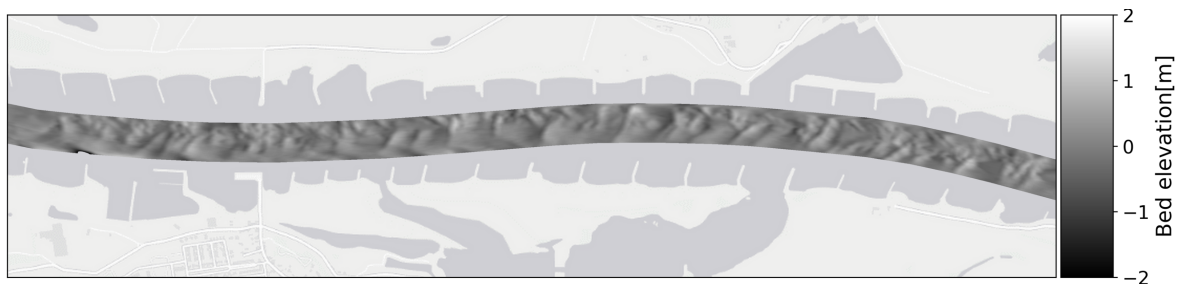


Figure 13: River bed based on MBES with a spatial resolution of 1x1 m at Druten in March 2019.

3.2.2 River dune analysis

The wavelet analysis of Lokin et al. (in prep.) was performed on the bed level measurements to extract the river dunes. The result of the wavelet analysis was the wavelet spectrum. The dune profile was reconstructed from the wavelet spectrum. The dune profile was used to determine the geometry of the river dunes. The dune celerity between two consecutive measurements was analysed with the cross-correlation technique.

Wavelet analysis

For this MBES data, the wavelet analysis was the most suitable to derive the river dune characteristics (Gutierrez et al., 2018). River dunes can also be manually determined in case of a small data set, as suggested by Blom et al. (2003). However, this research was dealing with a large data set. The wavelet analysis is a tool to analyse local variations of power within a time series (Torrence & Compo, 1998). The wavelet analysis is comparable to the Fourier analysis. However, the wavelet analysis develops a time series not only in frequency but also in time. This is an advantage since the bed measurements are nonstationary (Liu et al., 2007). For the wavelet analysis, the gridded MBES data was interpolated into line profiles (see Figure 14). The study area starts at the Tacticusbridge (upstream) and ends at the Prince Willem Alexanderbridge (downstream). The line profiles were 170 parallel lines over the length of the area of interest with the bed level profile. The outer 10 lines, ± 20 meters on both sides, of the river bed were not incorporated in the wavelet analysis because of the disturbed height profile due to the groynes. 150-line profiles were, therefore, considered that were approximately two meters apart.

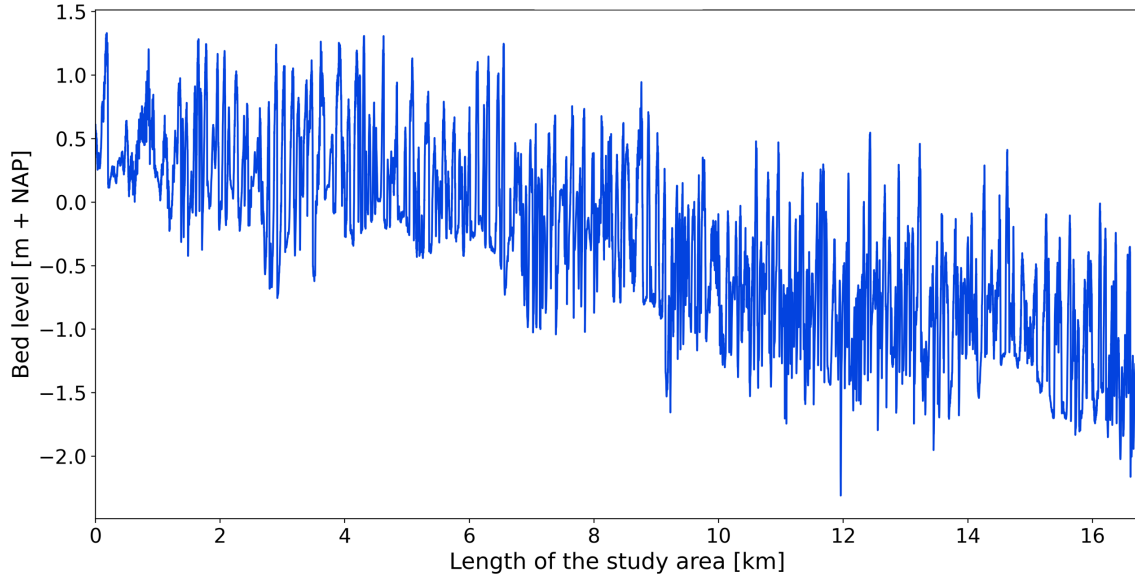


Figure 14: Graph of the line profile with the bed level over the length of the study area on 6 January 2020.

Next, the line profiles were analysed by a wavelet analysis with the Morlet wavelet. Guitierrez et al. (2013) state that the Morlet wavelet is the most efficient in retrieving small periodicities from bed forms. This wavelet function was, therefore, used in this wavelet analysis. The definition and a graph of the Morlet wavelet (Figure 15) can be seen below.

$$\psi_0(\eta) = \pi^{-\frac{1}{4}} e^{i\omega_0\eta} e^{-\frac{\eta^2}{2}} \quad (10)$$

- ψ_0 = wavelet function [-]
- η = non-dimensional time parameter [-]
- i = complex number [-]
- ω_0 = non-dimensional frequency [-]

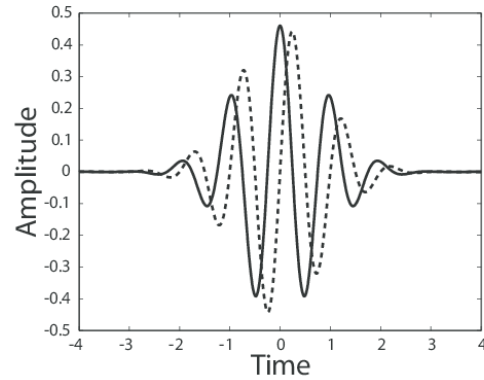


Figure 15: Morlet wavelet with real part (solid) and imaginary part (dashed) (Lancia, 2014).

The wavelet analysis with the Morlet wavelet produced a wavelet spectrum. Liu et al. (2007) observed that the wavelet spectra of Torrence & Compo (1998) were biased in favour of large-scale features. The wavelet scale indicates how stretched the Morlet wavelet is. The wavelet is very broad in frequency at small scales (high-frequency) and peaks in the spectrum get smoothed out. The wavelet is narrower in frequency at large scales (low-frequency) and peaks are larger and sharper. The energy is, therefore, smaller at small scales and high-frequency peaks tend to be underestimated. Comparison of the peaks for different scales is then not possible. The biased wavelet spectra can be corrected by a division of each energy value by the scale it corresponds (Liu et al., 2007).

Figure 16 shows the corrected wavelet spectrum for an approximately average water level (6.06 m + NAP) at Dodewaard. In the left subplot, the length of the study area is plotted against the wavelet scale. The energy increases with the darkness of the colour blue. The right subplot shows the power of the pattern (scale) by the global wavelet power.

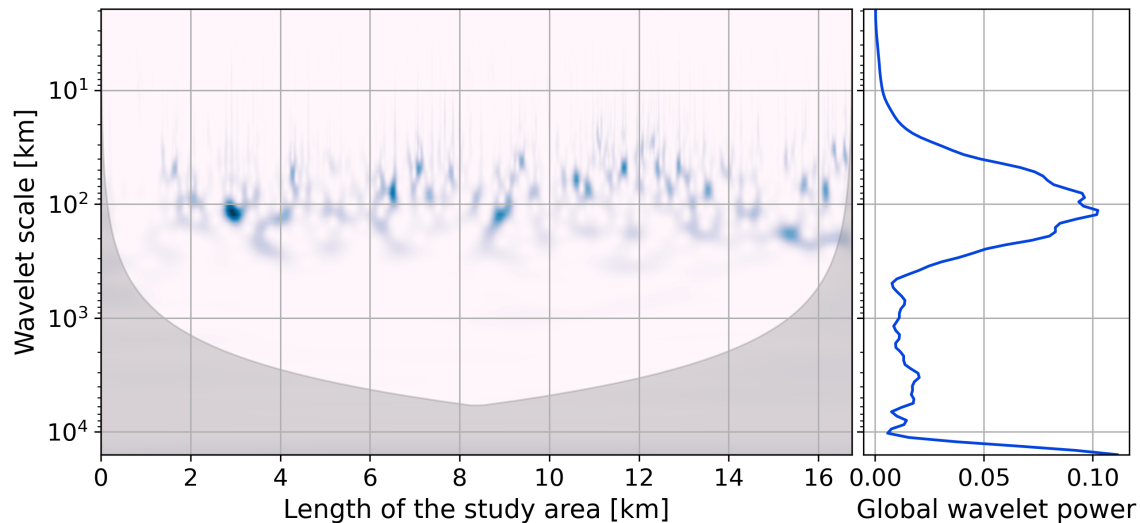


Figure 16: Wavelet spectrum for centreline of the Waal at Druten on 6 January 2020.

River dune geometry

The dune profiles were reconstructed from the wavelet spectrum by using representative dune length scales as a bandpass filter. Other bed forms or irregularities in the bed profile were excluded. De Ruijscher et al. (2020) studied the dune length for a stretch in the Waal that is also located in the study area of this research. De Ruijscher et al. (2020) found dune lengths of 10-200 meters, which is in line with the research of Julien et al. (2002). Wilbers & Ten Brinke (2003) found in their research a dune length between 10-40 meters at Beneden-Leeuwen in the Waal. The dune profile in this research was reconstructed by the wavelet scales between 20-300 meters. The lower limit was chosen at two times the theoretical length of ripples, 5 to 10 meters (Zomer et al., 2021), to make sure this bed form was excluded. By trial-and-error, the upper limit was chosen higher than the representative dune length to guarantee that the dunes were completely visible (Lokin et al, in prep.). Besides that, the chosen range of wavelet scales for the dune profile was also in accordance with the clear pattern that is visible in the wavelet spectrum in Figure 16.

The crests and the troughs of the dunes were found by using the reconstructed dune profile and the filtered bed signal. The filtered bed signal was determined by the Savitzky-Golay (S-G) filter. This filter was used to denoise the bed signal. The combination of the S-G filter with the wavelet analysis was also used in a different field of study by Samann & Schanze (2019). This resulted in a smoothing of the original bed profile in which only the primary dunes became visible. The dune peaks were found by the local maxima in the reconstructed dune profile. These locations of the dune peaks were plotted on the filtered bed signal. The dune crests were determined by the local maxima closest to each plotted dune peak on the filtered bed signal. The dune crests had at least a relative height of 0.1 meters to exclude other bed forms and higher-order dunes. The dune troughs were determined by the local minimum between the dune crests on the filtered bed profile (Lokin et al, in prep.). This method has led to the geometry of the river dunes.

River dune celerity

The migration rate of the river dunes was also analysed since sediment transport is also affected by navigation due to the velocities on the bed (Dorst et al., 2016; Ten Brinke et al., 2004). The MBES measurements were done almost every two weeks. The migration distance of the river dunes was determined between two successive measurements by using the spatial cross-correlation technique (Ten Brinke, Wilbers, et al., 1999). The spatial lag with the highest cross-correlation coefficient determined the displacement of the river dune between the consecutive measurements. The spatial cross-correlation was executed over the bed level profiles by sections of a 1000 meter to neglect large-

scale river morphodynamics (Lokin et al, in prep.). For this cross-correlation technique was assumed that the river dunes were always migrating downstream and the dune shape remained comparatively constant (Ten Brinke, Wilbers, et al., 1999). Finally, the migration of the river dunes was determined by dividing the displacement of the river dunes over the time difference between the two successive measurements.

3.3 Navigation

The signals of the AIS with the longitude and latitude of every ship were used to interpolate every ship track in the study area. All the ship tracks together determined the ship intensity for the river section.

3.3.1 AIS data

The second available data set contained detailed anonymous information about navigation by the AIS devices. AIS is used for communication at the waterway between ships, and between ships and traffic centers. This communication is necessary to increase safety. AIS systems are required in the Rhine branches since 1 December 2014. The ships were not obligated to have an AIS device onboard before this date (Rijkswaterstaat, 2021). The AIS device sends a signal almost every 30 seconds which results in an average monthly sample of 5 million signals. The following information was used from the AIS data: timestamp, longitude, latitude, course over ground (COG), speed over ground (SOG), maritime mobile service identity number (MMSI) and electronic reporting international code (ERI).

Observations showed a difference in sailing speed for the navigation directions. The mean navigation speed for up sailing ships (11.28 km/hr) was lower than for down sailing ships (17.76 km/hr). With an average speed of 15 km/hr, the signals are about 125 meters apart. The speed difference per navigation direction can be seen in the histogram in Figure 17. This effect disappeared if the flow velocity in the river was deducted from the speed of the down sailing ships and added to the speed of the up sailing ships. The average flow velocity was 0.92 m/s (3.31 km/hr) for July 2020, which resulted in an almost equal average speed for up sailing ships (14.59 km/hr) and down sailing ships (14.45 km/hr) (Vrijaldenhoven, personal communication, May 28, 2021). The difference in navigation speed per sailing direction was, thus, related to the flow velocity in the river.

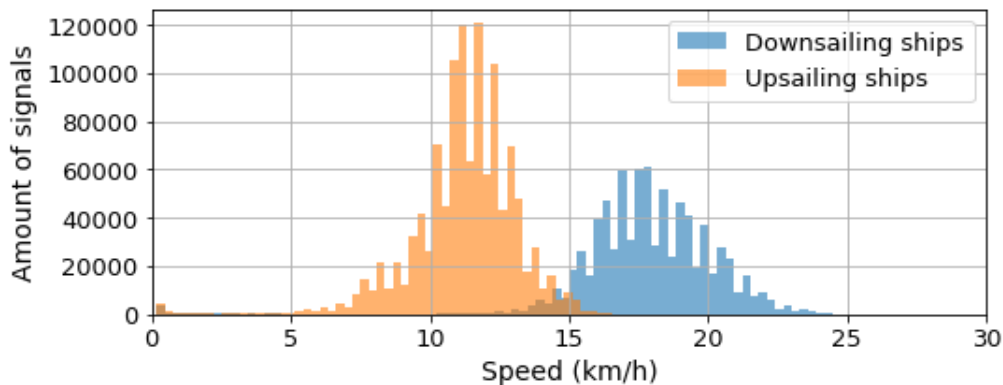


Figure 17: Histogram of the speed difference per navigation direction for July 2020.

3.3.2 Ship intensity analysis

The ship movement was analysed based on the AIS data set. This analysis was done in Python code using Jupyter notebook. The following packages were used: pandas, movingpandas, geopandas, cartopy, geoviews and holoviews. The first step was to make the AIS data set readable by converting the JSON format into a Parquet format. The Parquet format was more efficient for processing since it reduced the file size from approximately 4 GB to 200 MB. The second step was to filter the AIS data set. This analysis was only focusing on the ship movement within the specified river section in Waal. Data from adjacent harbours was, therefore, not taken into account. The data was also filtered on the values for the SOG. Data from stationary ships was excluded (SOG = 0 km/hr). The data was included

again as soon as the ship started sailing. Data with abnormal high-speed records were also removed (SOG > 30 km/hr). Therefore, the monthly data set was reduced to 2 million signals after the filtering.

Thereafter, it was possible to start processing the data. The third step was to group the data by the MMSI-number (the ship’s number). The fourth step was to determine the ship trajectories for each MMSI-number by the time delta. A new ship trajectory was created within the grouped data if five minutes no signal was registered. This resulted in different ship trajectories for each ship number. The fifth step was to generalise the data points per ship trajectory based on distance. The generalisation ensured that the data points were at least a minimum distance apart to reduce data per ship trajectory. The minimum distance between the locations of the data was set at 100 meters, by trial-and-error, which still resulted in smooth ship trajectories. Figure 18 shows the longitude and latitude of the generalised AIS signals for a ship track. With this method, about 300 – 500 ship tracks were recorded per day.

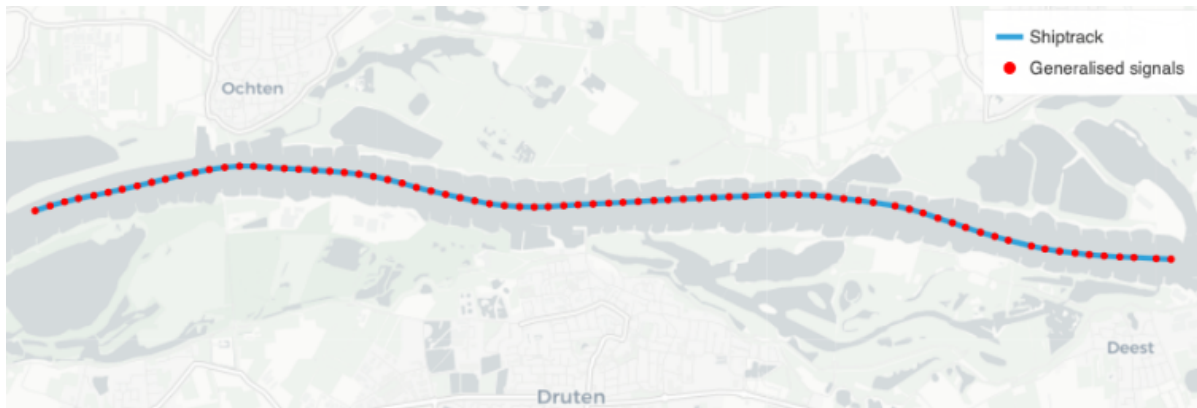


Figure 18: Map of AIS signals (red dots) within a single ship track (blue line) for the Waal.

The ship intensity analysis was used to determine a hexbin plot with all the ship tracks (shown in the next chapter). This hexbin plot could indicate the main ship tracks within the study area which can be filtered on navigation direction. Research has shown so far that downstream sailing ships normally follow the right bank and upstream sailing ships the left bank (seen from the discharge direction). This hypothesis can be tested with this ship intensity analysis.

All the steps are summarised below in Table 3. The script that was used in Jupyter Notebook can be seen in Appendix B: Script Jupyter Notebook ship intensity analysis.

Table 3: Steps taken in ship intensity analysis to determine ship tracks.

Step:	Action:
0	Downloading packages
1	Convert JSON-format to Parquet-format as dataframe
2	Filter data set on position and outliers in navigation speed
3	Group data by MMSI-number
4	Convert AIS signals to ship track
5	Generalise ship track

4 Results

The study aims to determine the effect of navigation on river dunes. However, multiple factors in the river, and not only navigation, determine the behaviour of the river dunes. The first paragraph focuses on the effect of water level (which is related to the discharge) on the geometry, celerity and pattern of the river dunes to analyse the general behaviour. The first paragraph is, therefore, used to validate the results of this research. The second paragraph describes the effect of navigation on the river dunes. Ships are different loaded per navigation direction, which results in different water movements per bank. This bank effect is analysed on the geometry and celerity of the river dunes and is related to the first research question. For the second research question, the geometry and celerity of the river dunes are analysed on ship intensity.

4.1 River dune behaviour

Changes in discharge result in both flow velocity and water depth changes. These two parameters determine the shear stress. The shear stress is the force of the flow per unit area acting on the river bed. Sediment gets into motion as soon as the shear stress is higher than the resistance of the sediment (Shields, 1936a; van Rijn, 1993). Changes in the water level (related to the water depth), thus, result in changes in the geometry and the celerity of the river dunes. Therefore, the general behaviour of the river dunes is analysed below.

Figure 19 shows the dune height and the dune length for the water level by quantitative analysis. The dune length is plotted on the left axis in red and the dune height is plotted on the right axis in blue. The values for the geometry of the river dunes are first averaged over the length and then the median is determined over the width of the river section. The median is chosen over the width of the river to put less emphasis on high values at the outer sides of the river. In Figure 19 is a clear trend of decreasing dune length observable for an increasing water level. The R-squared value shows a reliability of 0.80 for the trend line (red). The dune length varies approximately between 60 and 120 meters. The trend for the dune length is again noticeable for the dune height but in opposite direction. The dune height is, thus, increasing with the water level. However, the associated trendline is less reliable with a R-squared value of 0.65. The dune height changes between 0.55 and 1.05 meters. Thus, the results show a different trend for the dune length and dune height

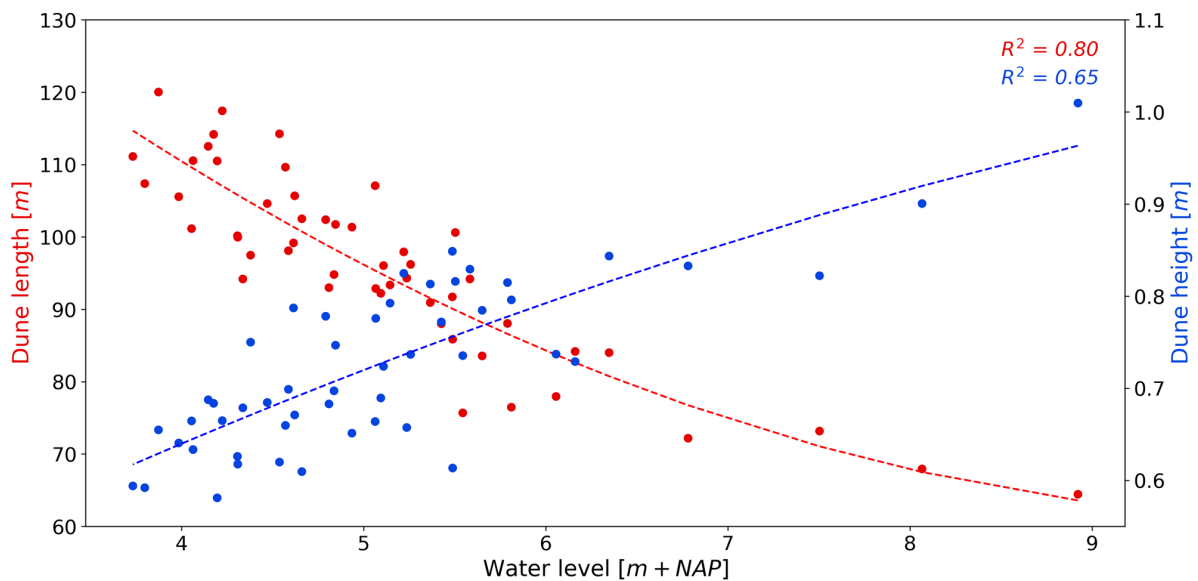


Figure 19: Dune height (blue) and length (red) for the water level at the Waal section Dodewaard-Ochten for 2019-2020 (average bed level is 0.25 m – NAP).

Cross-correlation, as discussed in the method, determines the migration rate of the river dunes. Figure 20 shows the median dune celerity for the water level over the length and width of the Waal section Dodewaard-Ochten for 2019-2020. The result is a trend of an increasing dune celerity for an increasing water level, but with a low R-squared value of 0.52 (blue dashed line). The dune celerity roughly varies between 3.0 and 7.0 m/day. The average values for the cross-correlation are visible by the colour in the scatterplot. As can be seen in Figure 20, not all the data points are even reliable due to the low cross-correlation values (light colours). Therefore, Figure 20 shows the median values for the dune celerity, instead of the mean values, to put less emphasis on dune celerity values with low cross-correlation values.

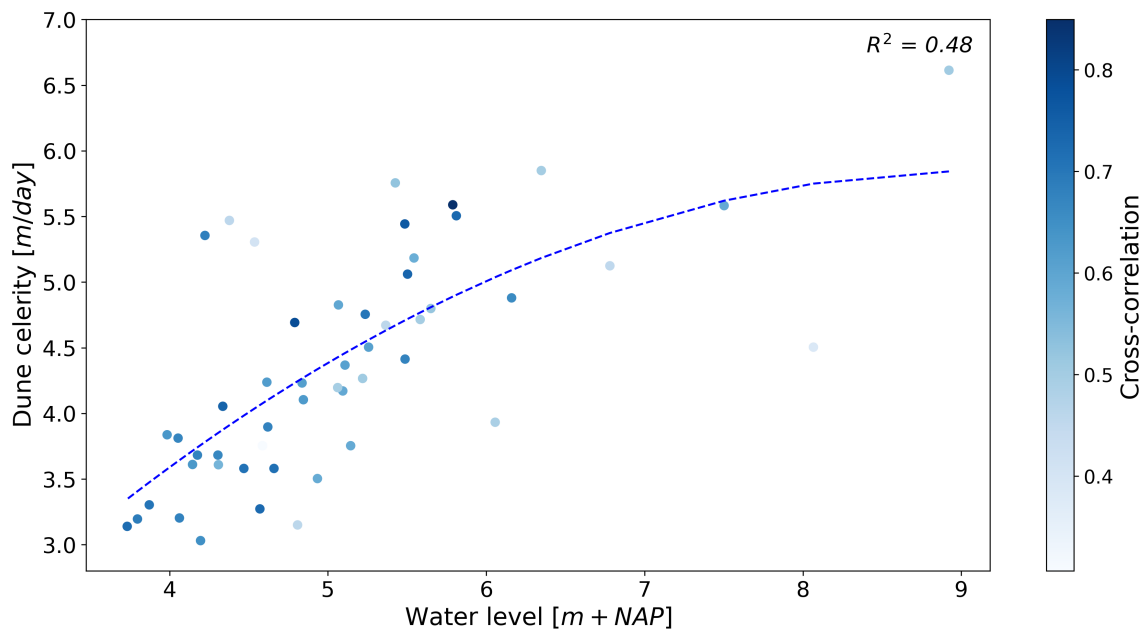


Figure 20: Dune celerity for the water level at the Waal section Dodewaard-Ochten for 2019-2020 (average bed level is 0.25 m – NAP).

Further analysis showed that the dune pattern is also clearly influenced by the water level. The visual results of the dune pattern are shown in Figure 21 and Figure 22. These Figures contain a map of the dune levels with respect to the mean bed level at the Waal section Druten. The dune crests are shown by a black line to present the dune pattern. The dune pattern is presented for different conditions. Figure 21 the dune pattern for 17-03-2020 during high water (8.92 m + NAP at Dodewaard) and Figure 22 for 07-08-2020 during low water (3.98 m + NAP at Dodewaard). Both dates have similar conditions at least a month in advance as during the measurement. What stands out in Figure 21 is the regularity in the dune crests. Almost all the crests are uniform lines over the width of the river. Compared to Figure 22, the dune pattern shows much more irregularity. Also, the results present a longer dune length during low water than during high water. Thus, the results show shorter dune lengths and a more regular pattern of the dune crests during high water.

Figure 21 and Figure 22 provide the dune pattern for a straight river section at Druten. A bend river section is also located within the study area at Beneden-Leeuwen. Appendix C shows the same Figures with the dune pattern but composed for Beneden-Leeuwen. These Figures show comparable results for the dune pattern between the two conditions. Interestingly, the dune crests are even more regular in the bend section than in the straight section during high water.

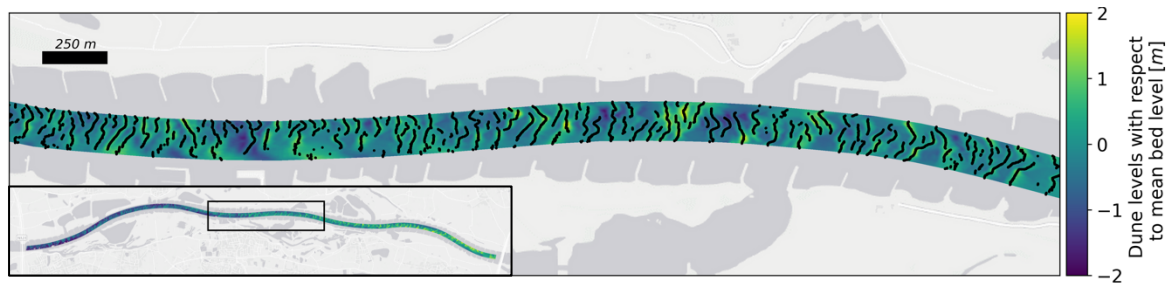


Figure 21: Dune pattern of the crests during high water at the Waal section Druten for 17-03-2020 (water level of 8.92 m + NAP for a bed level of 0.25 m – NAP at Dodewaard). The rectangle in the bottom left of the Figure indicates Druten in the study area.

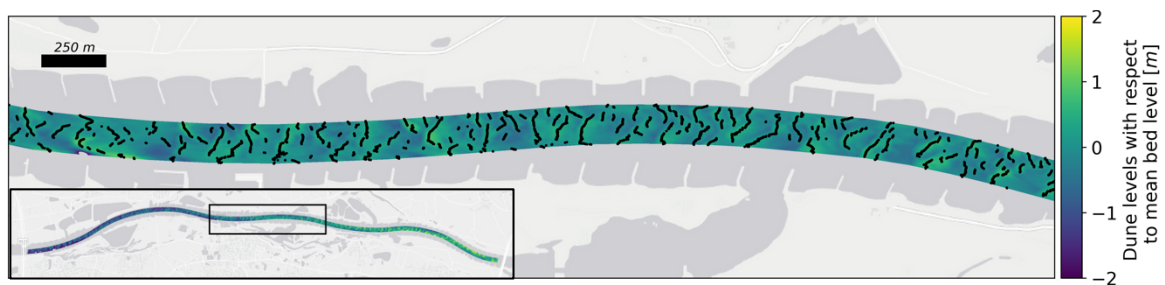


Figure 22: Dune pattern of the crests during low water at the Waal section Druten for 07-08-2020 (water level of 3.98 m + NAP for a bed level of 0.25 m – NAP at Dodewaard). The rectangle in the bottom left of the Figure indicates Druten in the study area.

4.2 Navigation

Navigation induces water movement which changes the flow conditions in the river. The difference in cargo, between up sailing (heavily loaded) and down sailing ships (less loaded), causes a variation in induced currents per bank (Wilbers & Ten Brinke, 2003). The first section analyses this bank effect on the geometry and celerity of the river dunes. This first section relates to the first research question. The second section identifies the primary navigation tracks over the river width and determines the effect of the navigation tracks on the geometry and celerity of the river dunes. This section also determines the effect of the ship intensity difference between 2019 and 2020 on the geometry and celerity of the river dunes. This second section relates to the second research question.

4.2.1 Bank effects

To compare the difference in river dunes between the banks, Figure 23 shows an overview of the dune length over the river width for the entire study area in the period 2019-2020. This is illustrated in the upper subplot. The second subplot presents the water level over time. Figure 23 shows again an increase in dune length for a decrease in water level, just as in Figure 19. Dune lengths vary between 54 and 216 meters. This range is much larger than in Figure 19 because the median values over the width of the river are no longer used. Surprisingly, the result shows much longer dune lengths at the outer sides of the river. In the middle section of the river, the dune lengths are much more constant between approximately 50 and 120 meters. Thus, the dune length behaves differently over the river width.

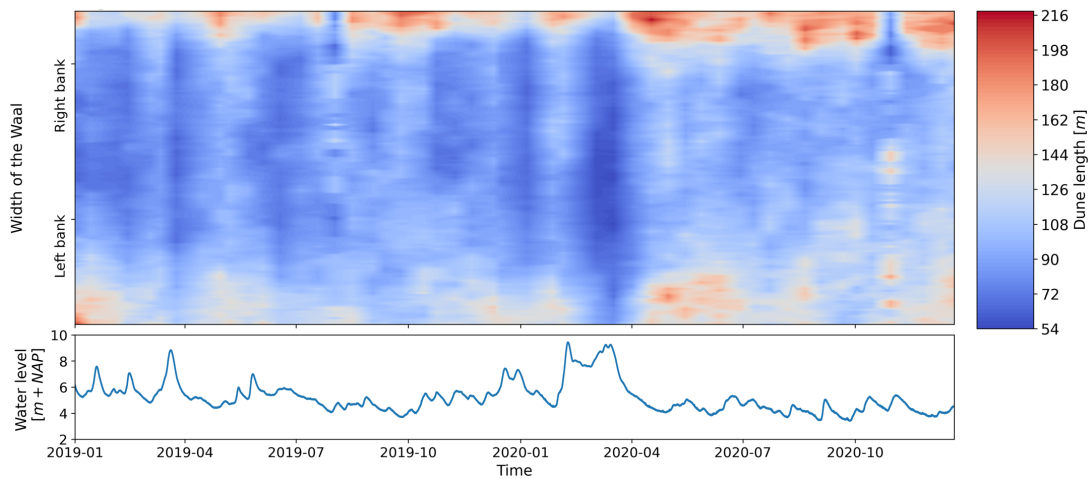


Figure 23: Dune length over the river width for the water level at the Waal section Dodewaard-Ochten for 2019-2020 (average bed level is 0.25 m – NAP). The bottom half of the Waal’s width is the left bank and the top half is the right bank (seen from the discharge direction).

Figure 24 presents the dune height over the river width for the water level at the Waal section Dodewaard-Ochten for 2019-2020. The range for the dune height is from 0.33 to 1.14 meters, which is also wider than detected in Figure 19. The trend in Figure 24 is comparable with the trend in Figure 19, which shows an increase in dune height with an increase in water level. However, this trend is visible over the entire width of the river instead of only at the outer sides. This result is somewhat counterintuitive in comparison to Figure 23. Figure 24 shows, thus, much more uniformity over the river width.

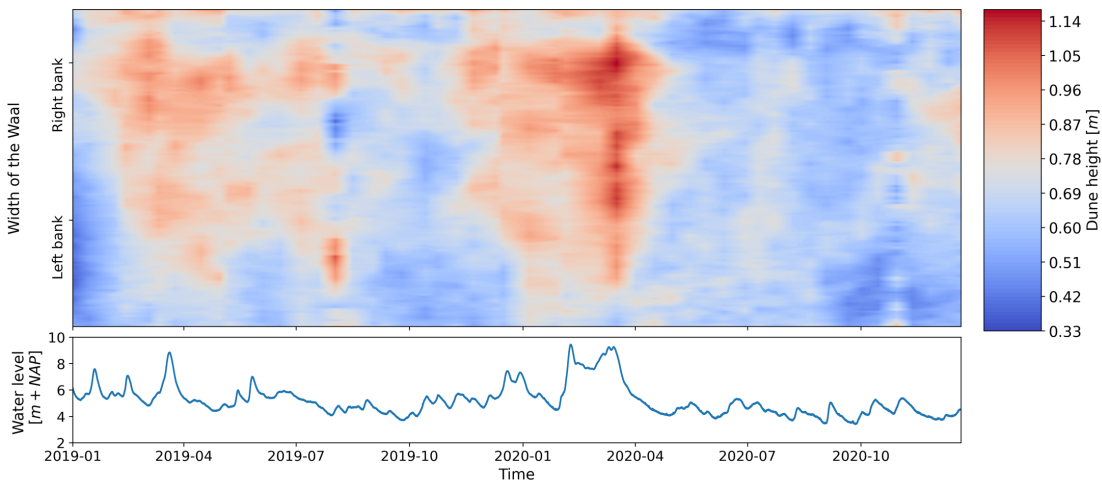


Figure 24: Dune height over the river width for the water level at the Waal section Dodewaard-Ochten for 2019-2020 (average bed level is 0.25 m – NAP). The bottom half of the Waal’s width is the left bank and the top half is the right bank (seen from the discharge direction).

The selected period of low water are the months July, August and September in 2019 and 2020. During a period of low water, the effect of navigation on the river bed increases since the keel-clearance decreases. However, the river doesn’t really adhere to the calendar. Therefore, the measurements are used between 2019-07-19 – 2019-10-14 and 2020-07-10 – 2020-09-21. Both time periods use six measurements of MBES data. These selected time periods have an average water level of 4.53 m + NAP (2019) and 4.26 m + NAP (2020). This change in the selected low water period of 2019 reduces the difference in water level which improves the analysis to compare both low water periods on the dune length, height and celerity.

Table 4 compares the median dune length and height for both selected low water periods in 2019 and 2020. A low water period results in longer dune lengths and smaller dune heights, as observed in the paragraph about the river dune behaviour. The right bank consists of lines 0 until 74 and the left bank consists of lines 75 until 149. The dune length is on average longer for the left bank (104.28 m) than for the right bank (95.53 m) for 2019 and 2020 combined. The difference in dune length for the left bank (Mean = 104.28 m; SD = 8.12 m) compared to the right bank (Mean = 95.52 m; SD = 5.74 m) is also significant ($t(22) = 3.05$; $p = 5.9 \cdot 10^{-3}$), by assuming at least a 5% level of significance. Observations show a higher dune height for the right bank (0.71 m) than for the left bank (0.67 m) in 2019. However, this trend is no longer observed in 2020 since the dune height is equal for the right bank and left bank. The values are, therefore, not tested on significant differences. Table 4 only shows a significant difference in dune length between the right and left bank.

Table 4: The median dune length and height for the right and left bank in comparison to the overall river width for both low water periods in 2019 and 2020 (average bed level is 0.25 m – NAP).

Date	Water level [m + NAP]	Dune length Right bank [m]	Dune length Left bank [m]	Dune length Overall width [m]	Dune height Right bank [m]	Dune height Left bank [m]	Dune height Overall width [m]
2019-07-19	5.07	94.72	90.12	92.89	0.79	0.75	0.78
2019-08-16	4.59	98.05	98.12	98.11	0.72	0.69	0.70
2019-09-02	4.81	84.78	95.88	93.02	0.69	0.68	0.68
2019-09-12	4.34	91.88	96.46	94.22	0.70	0.64	0.68
2019-09-25	4.05	102.13	100.42	101.18	0.70	0.64	0.66
2019-10-14	4.31	94.19	102.82	99.96	0.67	0.60	0.62
	4.53	94.29	97.30	96.57	0.71	0.67	0.69
2020-07-10	4.84	87.23	109.87	94.84	0.69	0.71	0.70
2020-07-23	4.47	94.07	108.00	104.62	0.69	0.67	0.68
2020-08-07	3.98	98.59	109.61	105.59	0.63	0.64	0.64
2020-08-21	4.31	97.60	110.77	100.19	0.62	0.63	0.63
2020-09-03	3.80	98.00	116.61	107.38	0.59	0.60	0.59
2020-09-21	4.20	105.05	112.72	110.53	0.58	0.57	0.58
	4.26	96.76	111.26	103.86	0.64	0.64	0.64

Table 5 shows the median dune celerity for the selected low water periods in 2019 and 2020. A low water period results in a low dune celerity based on the general behaviour in Figure 20. The average correlation is also given to determine the accuracy of the value for the dune celerity. The dune celerity is higher for the right bank (3.89 m/day) than for the left bank over 2019 and 2020, as can be seen from the data in Table 5. The difference in dune celerity for the right bank (Mean = 3.89 m/day; SD = 0.50 m/day) and the left bank (Mean = 3.76 m/day; SD = 0.50 m/day) is, however, not significant ($t(22) = 0.64$; $p = 0.53$).

Table 5: The median dune celerity for the right and left bank in comparison to the overall river width for both low water periods in 2019 and 2020 (average bed level is 0.25 m – NAP).

Date	Water level [m + NAP]	Dune celerity Right bank [m/day]	Dune celerity Right bank Correlation	Dune celerity Left bank [m/day]	Dune celerity Left bank Correlation	Dune celerity Overall width [m/day]	Dune celerity Overall width Correlation
2019-07-19	5.07	5.04	0.53	4.61	0.66	4.83	0.60
2019-08-16	4.59	3.97	0.26	4.61	0.35	4.04	0.31
2019-09-02	4.81	3.68	0.42	3.62	0.50	3.62	0.46
2019-09-12	4.34	4.15	0.69	3.85	0.79	4.05	0.74
2019-09-25	4.05	3.97	0.63	3.73	0.71	3.81	0.67
2019-10-14	4.31	3.71	0.53	3.50	0.59	3.61	0.56
	4.53	4.09	0.51	3.99	0.60	3.99	0.56
2020-07-10	4.84	4.23	0.55	4.23	0.68	4.23	0.62
2020-07-23	4.47	3.81	0.67	3.27	0.75	3.58	0.71
2020-08-07	3.98	4.10	0.59	3.64	0.68	3.84	0.63
2020-08-21	4.31	3.75	0.63	3.61	0.70	3.68	0.67
2020-09-03	3.80	3.12	0.66	3.43	0.73	3.20	0.69
2020-09-21	4.20	3.20	0.62	2.98	0.68	3.03	0.65
	4.26	3.70	0.62	3.53	0.70	3.59	0.66

4.2.2 Ship intensity effects

The purpose of the second research question is to determine the effect of ship movement intensity on the geometry and propagation of river dunes based on the ship position data from the AIS. The first analysis examines the impact of the navigation tracks on the river dunes. This impact on the river dunes is compared with a track where the least navigation is observed. The second analysis compares the effect of the navigation tracks on the river dunes for both years due to a difference in ship intensity between the years. This section relates to the second research question.

Effect navigation tracks

A hexbin plot of all the ship tracks determines the tracks with the most navigation in the Waal. Figure 25 shows the hexbin plot of the ship intensity at the Waal section Ochten for the selected low water periods in 2019 and 2020. After trial-and-error, 150 bins are chosen on the horizontal axis of the total study area. This corresponds with a bin size of around 70 meters. The darkness of the colour blue indicates the number of signals within the bin. The primary navigation tracks are indicated by the yellow colour in the plot. These tracks correspond with the lines 15-44 and 105-134 and have on average 3000 to 4000 signals within the bins. Observations show the least navigation at the outer sides of the river. However, these tracks are not chosen to reduce the effect of groyne fields on the river dunes. The track with the least navigation is, therefore, chosen in between the tracks with the most navigation. The track with the least navigation corresponds with the lines 60-89 and has on average 1000 to 2000 signals within the bins. The following results use the identified tracks with the most and least navigation.

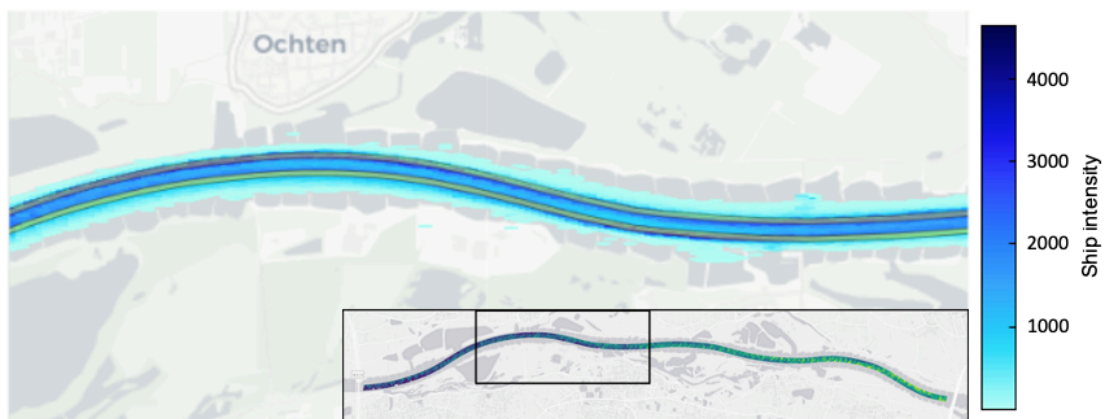


Figure 25: Hexbin plot of the ship intensity at the Waal section Ochten for the low water period in 2019-2020. At the bottom right, a map has been added to show where Ochten is located within the study area.

Table 6 compares the median dune length for the tracks with the most navigation and least navigation for the selected low water periods in 2019 and 2020. The primary navigation tracks correspond to the right and left track (seen from the discharge direction). The track with the least navigation corresponds to the middle track. The average dune length for the left track (108.05 m) is longer than for the right track (97.30 m) for the low water period. The dune length for the left track (Mean = 108.05 m; SD = 11.67 m) is even significantly longer than the right track (Mean = 97.30 m; SD = 5.85 m) based on the t-test ($t(22) = 2.85$; $p = 9.3 \cdot 10^{-3}$). Closer inspection of Table 6 shows a difference in dune length between the tracks with the most and the least navigation. The difference in dune length for the tracks with the most navigation (Mean = 102.67 m; SD = 10.56 m) and the least navigation (Mean = 92.65 m; SD = 4.99 m) is also significant again ($t(19) = 3.86$; $p = 1.1 \cdot 10^{-3}$). The dune length is, thus, significantly different between the navigation tracks but also between the tracks with the most and least navigation.

Table 6 also presents the dune height for the different tracks. The average dune height for the right track is higher than for the left track for both years. The difference in dune height between the right track (Mean = 0.70 m; SD = 0.08 m) and the left track (Mean = 0.64 m; SD = 0.06 m) is just significant ($t(22) = 2.08$; $p = 4.9 \cdot 10^{-2}$). The next chapter discusses whether this difference is caused by navigation. However, observations show almost no difference in the average dune height between the tracks with the most (0.67 m) and the least navigation (0.66 m). The difference is, therefore, not tested on significance. The dune height is, thus, only significant higher for the right track than for the left track.

Table 6: The median dune length and height for the tracks with the most and least navigation for both low water periods in 2019 and 2020 (average bed level is 0.25 m – NAP).

Date	Water level [m + NAP]	Dune length Right track [m]	Dune length Left track [m]	Dune length Middle track [m]	Dune height Right track [m]	Dune height Left track [m]	Dune height Middle track [m]
2019-07-19	5.07	93.91	93.52	87.46	0.85	0.75	0.79
2019-08-16	4.59	99.50	103.08	93.52	0.74	0.68	0.69
2019-09-02	4.81	88.43	94.22	89.06	0.73	0.66	0.71
2019-09-12	4.34	93.95	93.33	92.63	0.75	0.58	0.70
2019-09-25	4.05	104.14	100.22	96.57	0.78	0.58	0.66
2019-10-14	4.31	97.51	108.61	85.09	0.70	0.61	0.57
	4.53	96.24	98.83	90.72	0.76	0.64	0.69
2020-07-10	4.84	88.49	116.06	90.16	0.69	0.72	0.72
2020-07-23	4.47	93.71	107.62	95.39	0.68	0.65	0.70
2020-08-07	3.98	101.78	112.77	95.06	0.72	0.65	0.64
2020-08-21	4.31	101.86	130.16	88.14	0.62	0.65	0.60
2020-09-03	3.80	97.51	117.88	95.37	0.57	0.59	0.60
2020-09-21	4.20	106.86	119.07	103.30	0.62	0.58	0.57
	4.26	98.37	117.26	94.57	0.65	0.64	0.64

Table 7 provides an overview of the median dune celerity for the tracks with the most and the least navigation for the chosen low water period. The correlation is also again given to determine the accuracy of the dune celerity values. The dune celerity for the right track is higher than for the left track in both years. But the difference in dune celerity between the right track (Mean = 3.93 m/day; SD = 0.52 m/day) and the left track (Mean = 3.73 m/day; SD = 0.54 m/day) is definitely not significant ($t(22) = 0.92$; $p = 0.37$). The same can be observed between the tracks with the most and the least navigation. The dune celerity for the track with least navigation (Mean = 4.09 m/day; SD = 0.57 m/day) is higher than for the tracks with the most navigation (Mean = 3.83 m/day; SD = 0.53 m/day), but it is again not significant ($t(19) = 1.32$; $p = 0.2$). Therefore, the result shows no significant difference in dune celerity that could be related to navigation.

Table 7: The median dune celerity for the tracks with the most and least navigation for both low water periods in 2019 and 2020 (average bed level is 0.25 m – NAP).

Date	Water level [m + NAP]	Dune celerity Right track [m/day]	Dune celerity Right track Correlation	Dune celerity Left track [m/day]	Dune celerity Left track Correlation	Dune celerity Middle track [m/day]	Dune celerity Middle track Correlation
2019-07-19	5.07	5.11	0.50	4.47	0.66	5.04	0.61
2019-08-16	4.59	3.97	0.23	4.75	0.36	5.15	0.36
2019-09-02	4.81	3.80	0.37	3.68	0.49	3.74	0.50
2019-09-12	4.34	4.15	0.68	3.85	0.80	4.05	0.73
2019-09-25	4.05	4.35	0.60	3.73	0.72	3.89	0.66
2019-10-14	4.31	3.71	0.49	3.56	0.60	3.71	0.54
	4.53	4.18	0.48	4.01	0.61	4.26	0.57
2020-07-10	4.84	4.14	0.51	4.23	0.71	4.50	0.64
2020-07-23	4.47	3.89	0.63	3.12	0.76	3.81	0.71
2020-08-07	3.98	4.04	0.57	3.44	0.67	4.37	0.61
2020-08-21	4.31	3.75	0.62	3.61	0.70	3.83	0.63
2020-09-03	3.80	3.27	0.62	3.50	0.73	3.58	0.67
2020-09-21	4.20	3.03	0.59	2.86	0.67	3.36	0.65
	4.26	3.69	0.59	3.46	0.71	3.91	0.65

Effect navigation difference

This next analysis compares the difference in river dunes for the ship intensity over the years. Table 8 presents the ship intensity for the low water periods over the years 2019 and 2020. As discussed in the previous paragraph, the month October is added to the low water period of 2019. On average, observations showed more ship trajectories in 2019 than in 2020. The significance of this difference is tested for the average daily trajectories in periods of two weeks (same temporal resolution as the MBES data). The ship intensity for 2019 (Mean = 366.61; SD = 15.85) is then significantly higher than for 2020 (Mean = 313.70; SD = 21.69) based on the t-test ($t(10) = 6.01$; $p << 1.3 \cdot 10^{-4}$).

Table 8: Ship intensity for the low water period 2019-2020 (average bed level is 0.25 m – NAP).

	Water level 2019 [m + NAP]	Total trajectories 2019	Upsailing 2019	Downsailing 2019	Water level 2020 [m + NAP]	Total trajectories 2020	Upsailing 2020	Downsailing 2020
July	4.84	11374	5536	5838	4.51	9626	4594	5032
August	4.70	11015	5364	5651	4.06	9060	4307	4753
September	4.16	11266	5428	5838	3.95	10330	5055	5272
October	4.88	11288	5299	5989				

The geometry and celerity of the river dunes can be compared between the years by using Table 6 and Table 7 again. The dune length for the navigation tracks in 2019 (Mean = 97.54 m; SD = 5.73 m) is significantly shorter than the dune length for the navigation tracks in 2020 (Mean = 107.81 m; SD = 11.95 m) by using the t-test ($t(22) = 3.45$; $p << 2.3 \cdot 10^{-3}$). The dune height is not significant different between the navigation tracks in 2019 (Mean = 0.70 m; SD = 0.08 m) and the navigation tracks in 2020 (Mean = 0.65 m; SD = 0.05 m) ($t(22) = 1.84$; $p = 7.9 \cdot 10^{-2}$). Turning now to the dune celerity in Table 7, the difference in dune celerity between the navigation tracks in 2019 (Mean = 4.09 m/day; SD = 0.48 m/day) and the navigation tracks in 2020 (Mean = 3.57 m/day; SD = 0.45 m/day) is significant ($t(22) = 2.74$ $p = 1.2 \cdot 10^{-2}$). To summarise, the dune length and celerity shows a significant difference between 2019 and 2020.

Figure 26 presents a scatterplot of the dune length and celerity versus the corresponding water level to determine possible trends in the years. The left subplot shows the dune length and the right subplot shows the dune celerity. The red colour indicates the navigation tracks from 2019 and the blue colour indicates the navigation tracks from 2020. The left subplot shows a higher trendline for 2020 than for 2019. For the dune celerity, the right subplot presents a higher trendline for 2019 than for 2020. These trendlines correspond with the t-tests. Linear lines are chosen instead of horizontal lines to determine the trend with the water level.

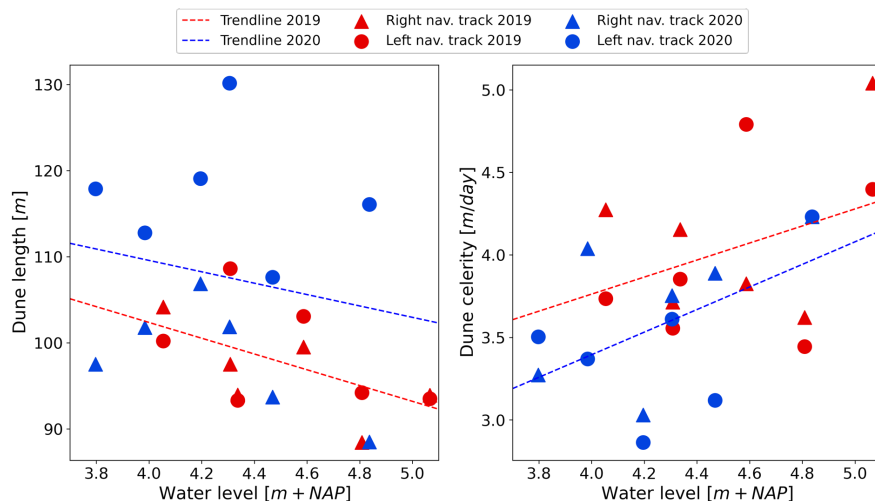


Figure 26: Dune length and celerity for the water level at the Waal section Dodewaard-Ochten for the low water periods in 2019-2020 (average bed level is 0.25 m - NAP). The red colour indicates the navigation tracks and trendline from 2019 and the blue colour indicates the navigation tracks and trendline from 2020. The triangles correspond with the right navigation track and the circles with the left navigation track.

The dune length and celerity can be estimated based on parameters by a multiple linear regression. The following parameters can be used for this analysis: water level and ship trajectories. Based on this multiple linear regression, the sensitivity of the parameters can be determined between the low water periods. For the dune length, the R-squared value is 0.45 for 2019 and 0.04 for 2020. For the dune celerity, the R-squared value is 0.13 for 2019 and 0.58 for 2020. The R-squared values shows that the multiple linear regressions are not really reliable. Nevertheless, a sensitivity analysis can still give some insight about the sensitivity of each parameter in the determination of the dune length and celerity. For the dune length, the sensitivity of the ship trajectories parameter increases from 2020 (0.02) to 2019 (0.36). However, the linear regression is much more sensitive to the water level parameter in 2019 (0.62) and 2020 (0.39). The sensitivity analysis for the dune celerity shows similar results. The linear regression is in both years more sensitive to the water level parameter (0.03 for 2019 and 0.05 for 2020) than to the ship trajectories parameter (0.00 for 2019 and 0.04 for 2020).

5 Discussion

This chapter discusses the results that are observed in the previous chapter. The first paragraph validates the general behaviour of the river dunes compared to other studies. The trend compared to the water level and the range of values express the general behaviour of the river dunes. The second paragraph discusses the effect of navigation on the geometry and celerity of the river dunes.

5.1 River dune behaviour

Shear stress characterises the general behaviour of the river dunes. Shear stress is the force of the water on the river bed. The shear stress changes if the water depth changes in the river (which is related to the discharge). The bed shear stress and the grain size determine the dune behaviour and the bed load transport. Wilbers & Ten Brinke (2003) argue that the grain size is, however, less important but probably determines the energy threshold for dune formation and the ability of the dune to respond to changing flow. The Shields mobility parameter (θ) takes the bed shear stress and grain size into account. The Shields mobility parameter can be determined by equation 4. Results of the Shields mobility parameter show reasonably good predictions for the dune height, length and migration during high discharges (Wilbers & Ten Brinke, 2003).

The geometry of the river dunes does not respond directly to the discharge due to hysteresis. The ratio between the dune volume and the bed load transport determines the response of the river dunes to the discharge variations (Ten Brinke, Wilbers, et al., 1999). Figure 19 also shows this response time by variations in data compared to the trend lines.

The sections below validate the results of this study for the geometry and celerity of the river dunes with other studies. Each section validates the trend compared to the water level and the range of values.

5.1.1 Dune length

Figure 19 shows a trend between the water level and the dune length. Contrary to the research of Wilbers & Ten Brinke (2003), Julien et al. (2002) and Van Rijn (1984c), the dune length decreases if the water level increases (increasing discharge). However, the studies of Wilbers & Ten Brinke (2003) and Julien et al. (2002) are only based on high water events (river floods). Fortunately, the trend in Figure 19 is in agreement with the trend observed by Lokin et al. (in prep.), Nieman et al. (2011) and de Ruijsscher et al. (2020). Lokin et al. (in prep.) and de Ruijsscher et al. (2020) showed a decrease in dune length during an increase in discharge. Nieman et al. (2011) presented the same trend by a decreasing dune length for an increasing force on the bed (Shields parameter). Figure 27 shows the results of this study. Niemann et al. (2011) explained this trend by the influence of gravity in the erosion fields as a diffusion term. During low flow, the forcing of the flow decreases and the influence of gravity (thus also diffusion) increases, which results in long and flat dunes as observed in Figure 19.

The range of values for the dune length in this study is in line with a recent study by De Ruijsscher et al. (2020). As mentioned in the method, the dune profiles were reconstructed from the wavelet spectrum. Representative dune length scales were, therefore, used as a bandpass filter, to exclude other bed forms. The following wavelet scale was used in order to reconstruct the dune profile: 10-300 meters. This wavelet scale was chosen based on research of De Ruijsscher et al. (2020), Wilbers & Ten Brinke (2003) and Julien et al. (2002). The median dune lengths in Figure 19 vary between 60 and 120 meters. Wilbers & Ten Brinke (2003) and Julien et al. (2002) described dune lengths for high water conditions which are not really in agreement with the wavelet spectra of this study. This discrepancy could be attributed to the difference in dune length trend. De Ruijsscher et al. (2020) found a similar trend in dune length as discussed above. The dune lengths in the wavelet spectra of this study are, therefore, in better agreement with the results of De Ruijsscher et al. (2020).

5.1.2 Dune height

Comparison of the findings in Figure 19 on dune height with those of other studies (Bradley & Venditti, 2017; de Ruijscher et al., 2020; Julien et al., 2002) confirms an increase in dune height with an increase in water depth. Julien et al. (2002) described that the height of the primary dunes varies between 0.1 and 0.6 meters during the flood in the Waal. The discharge increased from approximately 4000 to 9500 m³/s at Lobith during this flood, which results in a water level of almost 7.80 to 10.90 meters + NAP at Dodewaard (Rijkswaterstaat, 2018). According to Figure 19, the median dune height varies approximately between 0.6 and 1.0 meters for a water level range of 3.50-9.00 meters at Dodewaard. This result is not completely in line with the research of Julien et al. (2002). The result is more in line with the regression analysis of Bradley & Venditti (2017) and the dune predictors according to de Ruijscher et al. (2020). The scaling relation of Bradley & Venditti predicts a dune height range of 0.49 – 1.31. This dune height range is more in agreement with the observed dune height range in Figure 19. The dune predictor of Van Rijn (1984c) calculates a dune height of 0.64 meters for a below-median water depth and a dune height of 0.73 meters for an above-median water depth according to de Ruijscher et al. (2020). These dune heights are consistent with the data obtained in Figure 19. The trend and the range for the dune height are, thus, in accord with other studies.

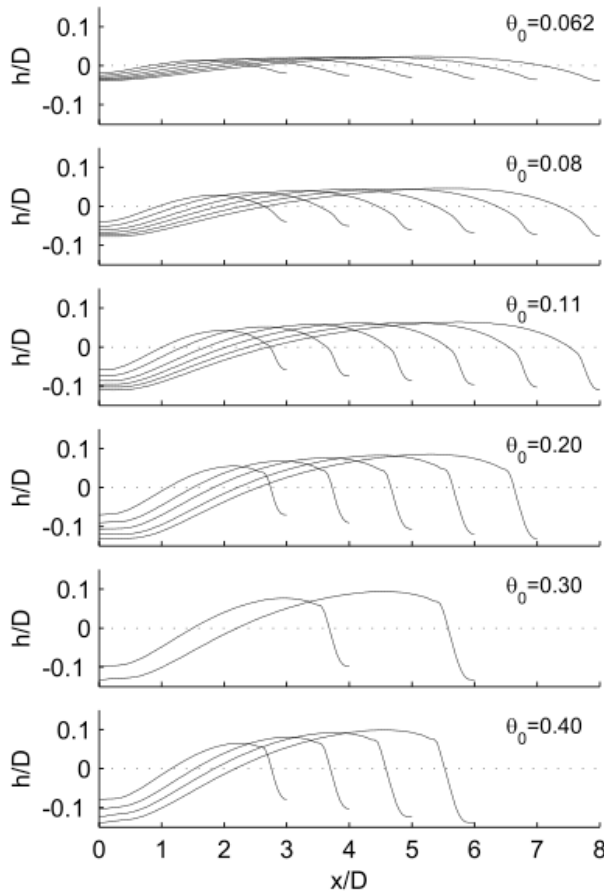


Figure 27: Equilibrium dunes calculated in a steady current for different forcing's (Niemann et al., 2011).

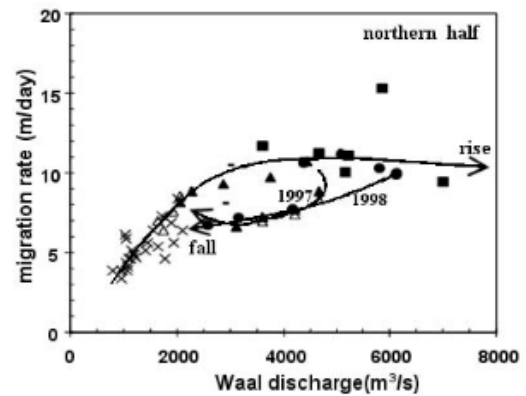


Figure 28: Dune migration rate for the Waal discharge at Beneden-Leeuwen during the floods of 1995, 1997 and 1998 (Wilbers & Ten Brinke, 2003).

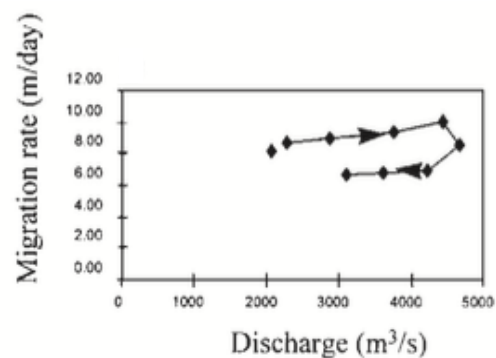


Figure 29: Dune migration rate for the discharge in the middle sand-bed section of the Waal during the flood of 1997 (Ten Brinke, Wilbers, et al., 1999).

5.1.3 Dune celerity

The trend in dune celerity is in agreement with other studies (Lokin et al., 2021; Ten Brinke, Wilbers, et al., 1999; Wilbers & Ten Brinke, 2003). Lokin et al. (2021) contributed to a conference with research into the evolution of primary dunes during low flows on the Waal. Results of this research showed that dunes are still migrating during low discharges of 800 to 1000 m³/s at Lobith (water level range of 3.25-3.75 meters + NAP at Dodewaard). The result of the median dune celerity versus the water level in Figure 20 confirms that dunes are still migrating during low water. Wilbers & Ten Brinke (2003) studied the dune migration at Beneden-Leeuwen in the Waal during the floods of 1995, 1997 and 1998. Migration rates were only determined for the primary dunes on the right bank of the river (seen from the discharge direction). Wilbers & Ten Brinke (2003) observed increasing migration rates during increasing discharges. Migration rates, however, stabilised around a discharge of about 3000 m³/s in the Waal. Figure 28 shows these results with the stabilisation. Ten Brinke, Wilbers, et al. (1999) observed the same trend in migration rate, which can be seen in Figure 29. The result in Figure 20 further supports this observation of an increasing dune celerity during an increasing water level. The dune celerity also seems to stabilize, but around a discharge of 3500 m³/s (water level of roughly 8.00 meters + NAP at Dodewaard). This stabilization is however difficult to determine accurately since no extreme high-water events occurred in 2019 and 2020. The stabilization in Figure 20 should, therefore, be interpreted with caution.

The median dune celerity ranges from 3 to 6 m/day according to Figure 20. The spatial cross-correlation technique between two successive measurements determined the dune celerity for this research. Wilbers & Ten Brinke (2003) found a different range for the dune celerity of 3 to 12 m/day during the floods of 1995, 1997 and 1998. This dune celerity range is probably higher because the observations were during floods with really high discharges which did not occur during 2019 and 2020. Zomer et al. (2021) show a dune celerity range of approximately 2 to 5 m/day for Tiel in 2018. The result in Figure 20 is roughly in accord with the findings of Zomer et al. (2021).

5.1.4 Dune pattern

Ten Brinke, Wilbers, et al. (1999) analysed the dune pattern for the upstream and downstream part of the middle sand-bed section in the Waal during the flood of 1997. In the upstream part, the dunes increased during the flood and the area was almost completely covered by dunes at the peak of the discharge. However, the pattern of the dunes had almost completely disappeared a week after the peak of the discharge. The downstream part showed different results. The river bed was already partly covered with a pattern of dunes at the start of the measurements, but this did not change anymore during the flood (Ten Brinke, Wilbers, et al., 1999). Figure 21 and Figure 22 show the dune pattern during high and low water. The dune pattern becomes more regular during high water and becomes more irregular during low water. The result of this research matches the findings for the upstream part of the middle sand-bed section in the Waal by Ten Brinke, Wilbers, et al. (1999).

5.1.5 Summary

Most of the field studies only focused on dune dynamics during high water events. This research presents the general behaviour of the river dunes for the period 2019-2020. The geometry and celerity of river dunes generally increase with an increase in water level according to multiple studies (Julien et al., 2002; Ten Brinke, Wilbers, et al., 1999; Wilbers & Ten Brinke, 2003). This research found similar trends apart from the dune length. Surprisingly, results showed an increase in the dune length during a decrease in water level. This trend can be explained by the increase in the influence of gravity and diffusion during low water (Niemann et al., 2011). The range of values for the geometry and celerity of the river dunes are reasonably consistent with other studies (Bradley & Venditti, 2017; de Ruijsscher et al., 2020; Ten Brinke, Wilbers, et al., 1999; Zomer et al., 2021). To summarise, the trend and range of the dune length, height and celerity of this research are in line with other studies.

5.2 Navigation

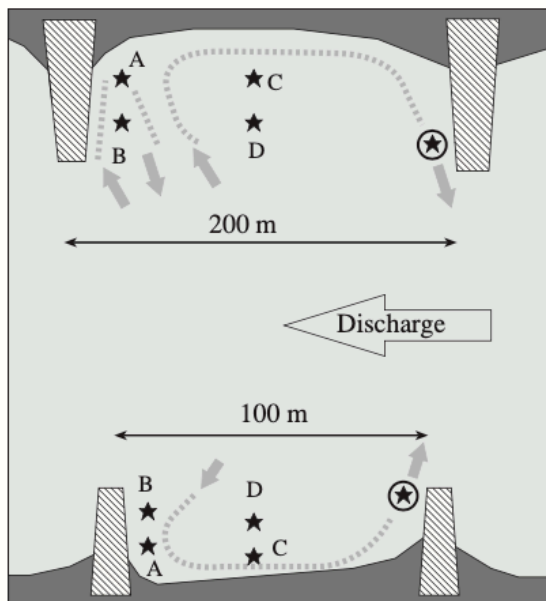
This section discusses the results of the second paragraph in the previous chapter. The bank effect (RQ1) and the ship intensity effect (RQ2) on the river dunes are both related to the river width. These results are, therefore, discussed for the river dune geometry and celerity in the first three paragraphs. The fourth paragraph discusses the effect of the ship intensity between the low water periods. The last paragraph discusses the practical applicability of the results.

5.2.1 Dune length

Figure 23 shows the average dune length over the river width for the period 2019-2020. This heatmap is used to show variations over the river width, which corresponds to the first research question. The observed average dune length varies between 54.30 and 217.67 meters in Figure 23. It is somewhat surprising that the dune length behaves clearly differently at the outer sides of the river.

The presence of groynes causes the different pattern in dune length at the outer sides of the river. According to Ten Brinke, Kruyt, et al. (1999), the flow pattern in the groyne fields produces scour holes (groyne erosion fields). The flow pattern for a small and a large distance between the groynes can be seen in Figure 30. For the small distance between the groynes, water flows into the groyne field at the downstream part and flows between the groynes to the upstream part. The water flows back into the main channel just downstream of the upstream groyne. Current velocities are high at this outflow point which results in scour holes. If the width between the groynes is 200 meters or more, a second circulation is produced just upstream of the downstream groyne. However, a second scour hole is generally not formed because the currents are not strong enough (Ten Brinke, Kruyt, et al., 1999). These results are measured with sensors attached to tripods in the groyne fields. The matching sediment transport volumes in perpendicular and parallel components are visible in Figure 31. Wilbers & Ten Brinke (2003) found similar results for the dune length at the outer sides of the river.

A North Bank



B South Bank

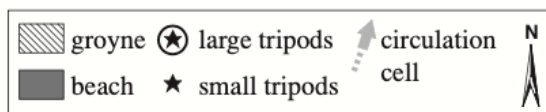


Figure 30: Flow pattern in the groyne fields with a large and small distance between the groynes (Ten Brinke, Kruyt, et al., 1999).

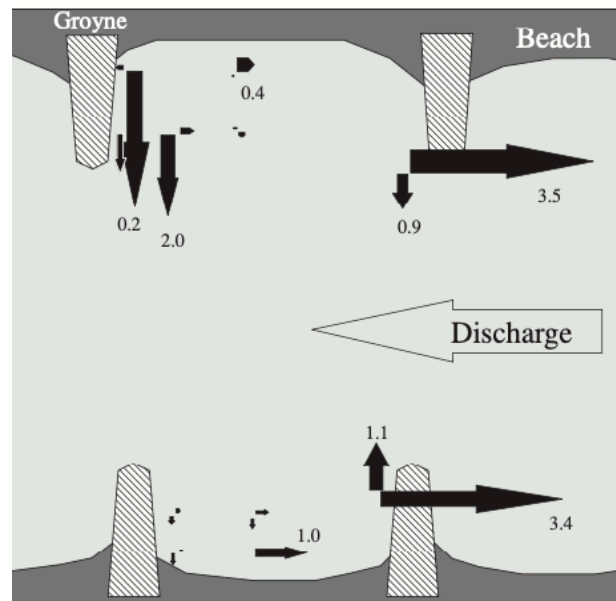


Figure 31: The sediment transport volumes in kg/s for groyne fields with a large and small distance between the groynes (Ten Brinke, Kruyt, et al., 1999).

River shoals form between the scour holes. The river bed is slightly higher in between the scour holes, which corresponds with a length of approximately the width between the groynes (± 200 meters). The river shoals affect the dune length results at the outer sides of the river. The size of the scour holes determines how far the dune length results are affected by the river shoals in the main channel (Ten Brinke, Kruyt, et al., 1999). In Figure 23, the dune lengths of 200 meters are especially noticeable at the right bank (dark red). The dune lengths are shorter at the left bank with lengths of about 160 meters (light red). The pattern that seems to be influenced by the groynes (red colour at the outer sides of the river) is, however, further visible into the main channel on the left bank. Thus, the scour holes affect the dune length results more on the left bank.

Navigation affects the hydrodynamics in the groyne fields according to Ten Brinke, Kruyt, et al. (1999) and Ten Brinke et al. (2004). Navigation induces water movement in the river by waves, currents and turbulence. The effect of this induced water movement increases during a decrease in discharge (Ten Brinke, Kruyt, et al., 1999). The primary wave consists of a front wave (in front of the ship), a stern wave (behind the ship) and in between a water level depression. Water flows from the bow wave (return flow) and stern wave (follow flow) to the water level depression (Ten Brinke et al., 2004). The water movement induced by navigation interacts with the flow pattern in a groyne field. Figure 32 shows this interaction step-by-step during a ship passage. Ten Brinke et al. (2004) used an upsailing barge-tow for a typical situation in the Waal with groynes that are 200 meters apart. The left figures show the acceleration and deceleration of the flow and the right figures show the matching flow pattern in Figure 32. As soon as the bow of the ship passes the groyne, the flow in the upstream groyne field is sucked along by the return flow of the ship (step 1). The eddy in the downstream groyne field disappears and the eddy in the upstream groyne field loses strength (step 2). The return flow stops at the stern of the ship. Behind the stern of the ship, the direction of the flow is changed by the follow flow. The follow flow refills the groyne fields in the opposite direction of the discharge as soon as the ship passes the groyne (steps 3-4). By the time the ship passes the next groyne, the follow flow (just downstream of the groyne) meets the return flow (just upstream of the groyne). This combination of flows strengthens the eddy just downstream of the groyne and produces the strongest currents induced by a ship's passage (step 4). As soon as the ship passes the groyne, the follow flow refills the next groyne field (step 5) (Ten Brinke et al., 2004). The effect of navigation on the hydrodynamics in the groyne field varies with the characteristics of the groyne field and the ship's passage.

The location of the groyne field with respect to the river is the most important parameter of the groyne field. At the inner (convex) bank the groyne fields are not really affected by navigation as these groyne fields are part of the point bar (area of deposition). Navigation has also not much impact on the outer (concave) bank since the river flow mainly determines the hydrodynamics in these groyne fields due to the high velocities. Based on the characteristics of the groyne field, navigation has the most effect on the hydrodynamics of the groyne field in straight river sections (Ten Brinke et al., 2004).

The most important parameters of the ship's passage that determine the effect on the groyne field hydrodynamics are the passing distance from the bank and the underwater volume of the ship according to Ten Brinke et al (2004). Ships need to pass the groynes at a relatively large distance to ensure enough keel-clearance. Of course, the impact of navigation on the hydrodynamics in the groyne field decreases as the passing distance from the bank increases (Ten Brinke et al., 2004). The effect of the underwater volume of the ship is reflected in the scour hole difference per bank. As already explained in the background, up sailing ship towards the Ruhr area are heavily loaded and down sailing ships toward the Port of Rotterdam are considerably less loaded. Up sailing ships often follow the left bank and down sailing ships the right bank (Ten Brinke et al., 2004; Wilbers & Ten Brinke, 2003). The difference in cargo results in a different keel-clearance and underwater volume of the ship. The ships with the smallest keel-clearance induce the strongest currents. Heavily loaded up sailing ships along the left bank, therefore, have more impact on the hydrodynamics of the groyne fields than significantly less loaded down sailing ships along the right bank. As a result, more erosion takes place at the left bank than at the right bank (Ten Brinke et al., 2004; Wilbers & Ten Brinke, 2003).

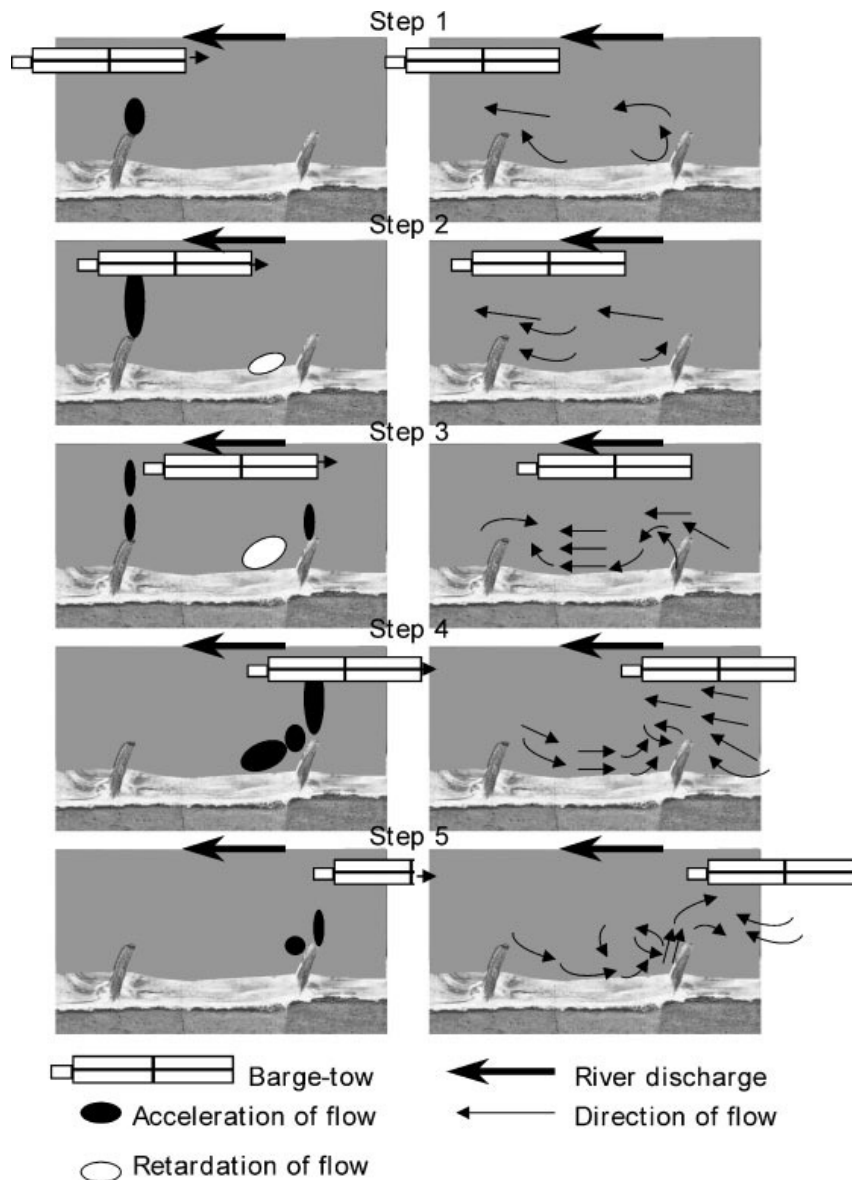


Figure 32: The interaction in flow between a ship and a characteristic groyne field along the Waal. The acceleration and deceleration of the flow (left) and the corresponding flow pattern (right) is visible during the passage of a ship (Ten Brinke et al., 2004).

This study presents longer dune lengths on the left bank than on the right bank as can be seen in Table 4. This result may be explained by the fact that scour holes are larger and further located into the main channel on the left bank since up sailing ships have more impact on the hydrodynamics in the groyne fields. Dunes are, therefore, affected by the river shoals further into the main channel (over a greater river width) at the left bank resulting in longer dune length results at the left bank compared to the right bank.

Navigation also affects the dune length in the navigation tracks. Figure 33 illustrates the navigation tracks (dashed lines) and navigation direction (arrows) over the river width. The area of influence of the groins is visible in both navigation tracks (red colour), but almost not anymore in the middle track (in between the navigation tracks). The dune length is, therefore, significantly longer in the navigation tracks than in the middle track as presented in Table 6. The area of influence of the groins is more visible in the left navigation track than in the right navigation track. Table 6 also shows significantly longer dune length results in the left navigation track. These observations may support the explanation that scour holes differ in size per bank. The dune length results at the outer sides of the river are, thus, likely related to navigation.

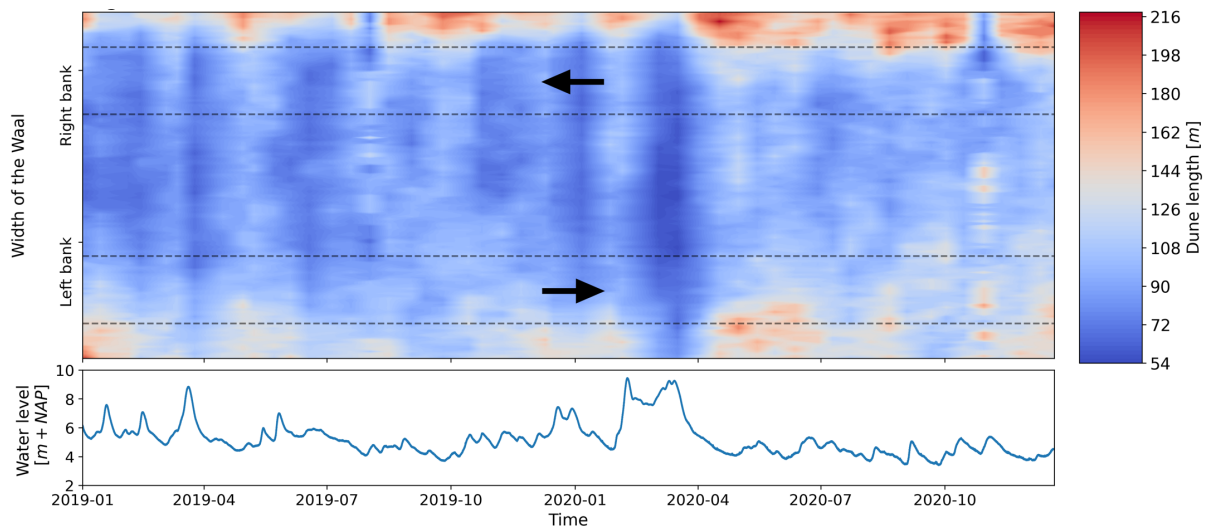


Figure 33: Dune length over the river width for the water level at the Waal section Dodewaard-Ochten for 2019-2020 (average bed level is 0.25 m – NAP). The bottom half of the Waal's width is the left bank and the top half is the right bank (seen from the discharge direction). The dashed lines indicate the navigation tracks and the arrows indicate the navigation direction.

5.2.2 Dune height

Dune height differences related to navigation are not found in Figure 24, Table 4 and Table 6. In this research, dune height shows more uniformity over the river width. Figure 24 shows a dune height range of 0.34-1.17 meters. The only observed significant result is a higher dune height at the right navigation track than at the left navigation track as can be seen in Table 6. This difference is however only observed during the low water period in 2019. During the low water period in 2020, the bank with the highest dune height differs per measurement. The results, thus, show no clear trend in dune height related to navigation. However, Wilbers & Ten Brinke (2003) found different dune heights for the right and the left bank for the Waal section at Beneden-Leeuwen for the floods in 1995, 1997, and 1998. The dunes were much higher for the left bank than for the right bank (Wilbers & Ten Brinke, 2003). Dorst et al. (2016) monitored and analysed the under-keel currents and the subsequent bed erosion in the Juliana Canal. The currents induced by navigation caused a 5-meter-wide erosion path. The erosion path deepened by 1 to 2 cm with every 10 ship passages. Comparable results were found by Robijns (2014), by a dune crest reduction of 25% for 10 ship passages. Thus, the results for the dune height related to navigation are not comparable with other studies.

It is possible, therefore, that the temporal effect of a single vessel with a really small under-keel clearance is much bigger than the overall effect of all the vessels. According to experts of Deltares and Rijkswaterstaat, dredge vessels of the contractor sometimes deliberately 'plough' through the river bed during low water to locally lower the river bed by turbulence. This 'ploughing' temporarily increases the under-keel clearance (Verbeek, personal communication, January 13, 2021). A further study with more focus on the dune height is, therefore, suggested. CoVadem data can be used for this further study to get direct measurements underneath the ship. Thus, the CoVadem data could gain insight into the local effect of navigation on the dune height.

5.2.3 Dune celerity

The difference in dune celerity per bank is probably not related to navigation. Table 5 shows that the dune celerity is higher at the right bank than at the left bank during the low water period. This difference in dune celerity may be due to the bend at Beneden-Leeuwen. The study area is almost completely straight, apart from the bend to the left at Beneden-Leeuwen. The velocity is the highest near the outer bank in a bend. The outer bank corresponds to the right bank in the bend at Beneden-Leeuwen. The dune celerity is, therefore, higher at the right bank since dune migration is related to the flow conditions (Ten Brinke, Wilbers, et al., 1999; Wilbers & Ten Brinke, 2003). This trend is however not significant due to the high variance, just as the other comparisons over the river width.

The MBES measurements were executed almost once per two weeks. On average, the dune migrates 60 meters in between two measurements, which is of the same order of magnitude as the dune length. The dune displacement is hard to determine accurately with this measurement frequency, which results in a high variance (Lokin et al., in prep.). In future research, it is recommended to use a data set with a higher sampling rate to obtain potentially significant results.

5.2.4 Navigation difference between the years

The dune length, height and celerity are also analysed between the years due to the significant difference in ship intensity. On average, almost 50 more ship passages per two weeks were observed during the lower water period in 2019 compared to 2020 (increase of 17%). The results show significant differences in the dune length and celerity. The trendlines of the dune length and celerity against the water level in Figure 26 are in agreement with the trendlines in Figure 19 and Figure 20.

According to section 5.2.1, navigation affects the dune length results by the river shoals. Heavily loaded ships cause larger scour holes (further located into the main channel) resulting in longer dune length results. It is, therefore, likely that more navigation would also lead to longer dune length results. However, Figure 26 is contrary to this explanation since the dune length results are longer for 2020 than for 2019. This rather contradictory result may be due to no information is available about the most important parameters of the ship's passage that determine the effect on the groyne field hydrodynamics. Ship intensity does not provide information about the underwater volume of the ship. Therefore, CoVadem data should be used to determine the underwater volume of the ships to quantify the effect of navigation on the dune length.

Navigation induces water movement and, therefore, also sediment transport. According to Appendix A, a single ship passage causes a bed load transport increase almost ten times greater than during natural flow. More sediment transport probably leads to a higher dune celerity. Figure 26 further supports the idea of an increase in dune celerity for an increase of ship intensity.

Nevertheless, the graphs in Figure 26 are more like a point cloud rather than a trend difference between the years. Therefore, the 'significant' differences for the dune length and celerity are rather related to the difference in water level between the years. The sensitivity analysis on the parameters of the multiple linear regressions also confirms this explanation. The low water period in 2019 (4.52 m) has a higher average water level than the low water period in 2020 (4.26 m). This difference in water level results in a shorter dune length in 2019 than in 2020 according to Figure 19. Figure 20 shows the opposite trend which results in a higher dune celerity in 2019 than in 2020. These overall trends are in line with the statistical differences for the dune length and celerity in Figure 26. Figure 26 most likely shows point clouds for both graphs due to hysteresis. An effect of ship intensity on the geometry and celerity of the river dunes is not excluded by this research. However, the effect of hydraulic conditions is probably stronger than the effect of ship movement for this ship intensity difference.

5.2.5 Practical applicability

This research suggests that navigation has no direct effect on the geometry and celerity of the river dunes. Results only showed an indirect effect of navigation on the bed at the outer sides of the river. These findings may be explained by the fact that navigation affects the hydrodynamics in the groyne fields and, thus, also the size of the scour holes and the river shoals. The river shoals in between the scour holes are, therefore, affecting the dune length results at the outer sides of the river. This effect of navigation on the hydrodynamics in the groyne field can be related to the underwater volume of the ship. As already mentioned, the CoVadem data gives insight into the underwater volume of the ship. In future work with the CoVadem data, it might be possible to quantify the effect of navigation on the size of scour holes and river shoals. This quantification improves knowledge about river bed management and river dune analysis.

This study suggests that no significant differences in dune celerity are caused by navigation. However, further research with CoVadem data could provide new insights. Since dune celerity is related to sediment transport, this research recommends to not include a navigation factor in transport equations based on these results.

6 Conclusions and recommendations

The purpose of this study was to determine the effect of inland navigation on the geometry and celerity of river dunes. Two research questions are used to fulfil the purpose of this research. The conclusions per research question are given below with some recommendations.

6.1 Conclusions

Research question 1: What are the differences in river dune geometry and celerity for the right and the left bank for a straight river section based on the MBES of the Waal?

The hypothesis is that up sailing ships along the left bank are heavily loaded and down sailing ships along the right bank are significantly less loaded. This bank effect on the river dunes is determined over the river width for the Waal section at Druten for low water periods in 2019 and 2020. The dune length behaves clearly different at the outer sides of the river. This result supports the idea that groynes affect the dune length results at the outer sides of the river. Navigation affects the groyne field hydrodynamics and, thus, also the scour holes. The passing distance and the underwater volume of the ship predominantly determine the effect of navigation on the groyne field hydrodynamics. The underwater volume of the ship is different per navigation direction due to the cargo difference per navigation direction. Up sailing ships are, therefore, likely to have more impact on the hydrodynamics in the groyne field which causes scour holes that are larger and further located into the main channel at the left bank. River shoals in between the scour holes affect the dune length results. Results of this study confirm that dune lengths are longer on the left bank (more affected by river shoals) than on the right bank (less affected by river shoals). Dune height shows more uniformity over the river width. Observations of the dune height showed no clear trend that could be related to navigation. The dune celerity showed a trend with higher values for the right bank than for the left bank. This difference is probably related to the high velocities near the outer bank (right bank) in the bend at Beneden-Leeuwen. However, a limitation of this study is that the trend is not significant due to the high variance in the data. The high variance is a result of the inaccuracy in the determination of the dune displacement. Based on these conclusions, only the dune length showed significant differences between the banks and this difference is indirectly related to navigation.

Research question 2: How is the geometry and propagation of river dunes affected by ship movement intensity based on the ship-position data from the AIS of the Waal?

The effect of ship movement intensity was analysed over the river width and between the low water periods. The geometry and celerity of the river dunes was first analysed over the river width. Navigation indirectly affects the dune length results in the navigation tracks by the groins. Observations showed again longer dune lengths in the left navigation track than in the right navigation track due to probably the cargo difference per navigation direction. Results showed again no effect of navigation in the height and celerity of the river dunes in the navigation tracks. The ship intensity was also analysed between the low water periods of 2019 and 2020. In the low water period of 2019 were 17% more ship trajectories observed than in the low water period of 2020. Observations showed significant differences between the years for the dune length and celerity. However, the graphs for the dune length and celerity are rather a point cloud than a trend difference. The significant differences are, therefore, rather related to the water level difference between the years. The effect of hydraulic conditions on river dunes is, thus, stronger than the effect of ship movement for this ship intensity difference.

Research aim: To quantify the effect of inland navigation on the geometry and celerity of river dunes to improve river bed management.

This study has not found any direct effect of navigation on the geometry and celerity of the river dunes. Only an indirect effect of navigation was observed on the length of the river dunes due to the impact of navigation on the hydrodynamics in the groyne fields. This effect of navigation is related to the underwater volume of the ship, and not ship intensity. The indirect impact of navigation on the dune length is, therefore, not quantified since this parameter is not known.

The hypothesis of this research was that the return current and turbulent propeller jets, induced by navigation, would affect the geometry and celerity of the river dunes. However, this effect is not observed by this ship intensity analysis. Nevertheless, no effect of ship intensity on the river dunes cannot be concluded since no field measurements of the bed level are available with no navigation.

6.2 Recommendations

Findings of this research did not show any direct effect of navigation on the geometry and celerity of the river dunes. Further work with CoVadem data needs to be done to establish whether the geometry and celerity of the river dunes is really not affected by navigation. CoVadem data are direct depth measurements underneath the ship. However, not all the ships have joined CoVadem so far. CoVadem data contains approximately 40 ships per month, while nearly 2500 ships per month are observed in the river section. Progress is, therefore, still needed to involve more ships. Nevertheless, CoVadem data could give insight into the underwater volume of the ship (related to under keel-clearance). Especially, the ships with a really small under keel-clearance are interesting since these ships produce the strongest currents. In future work with CoVadem data, it might be possible to quantify the effect of under keel-clearance on the geometry and celerity of river dunes.

Another advantage of the CoVadem data is the sampling rate. The temporal resolution of the MBES data is roughly two weeks. With this measurement frequency for the MBES data, the dune displacement is hard to determine accurately which results in a high variance. The CoVadem data are direct measurements underneath the ships. Therefore, riverbed measurements are more frequently available for the CoVadem data than for the MBES data. With this CoVadem data, the dune displacement can be determined more precisely. A possible effect of navigation on dune celerity can, thus, also be determined more accurately. Therefore, future work using the CoVadem data could yield new insights on the effect of navigation on dune celerity.

References

- Rijnvaartpolitierglement art. 11.01. (1995). <https://wetten.overheid.nl/BWBR0006923/2018-12-01>
- Abdel-Fattah, S., Amin, A., & Van Rijn, L. C. (2004). Sand Transport in Nile River, Egypt. *Journal of Hydraulic Engineering*, 130(6), p. 488–500. [https://doi.org/10.1061/\(asce\)0733-9429\(2004\)130:6\(488\)](https://doi.org/10.1061/(asce)0733-9429(2004)130:6(488))
- Allen, J. (1968). The accumulation of sediment in the lee of ripples and dunes, and the thickness of bottomset deposits. *Geological Magazine*, 105(2), p. 166–176. <https://doi.org/10.1111/j.1365-3091.1968.tb01110.x>
- Bisantino, T., Gentile, F., Milella, P., & Liuzzi, G. T. (2010). Effect of Time Scale on the Performance of Different Sediment Transport Formulas in a Semiarid Region. *Journal of Hydraulic Engineering*, 136(1), p. 56–61. [https://doi.org/10.1061/\(asce\)hy.1943-7900.0000125](https://doi.org/10.1061/(asce)hy.1943-7900.0000125)
- Blom, A., Ribberink, J. S., & de Vriend, H. J. (2003). Vertical sorting in bed forms: Flume experiments with a natural and a trimodal sediment mixture. *Water Resources Research*, 39(2), p. 1025. <https://doi.org/10.1029/2001WR001088>
- Bradley, R. W., & Venditti, J. G. (2017). Reevaluating dune scaling relations. *Earth-Science Reviews*, 165, p. 356–376. <https://doi.org/10.1016/j.earscirev.2016.11.004>
- Brownlie, W. B. (1981). Prediction of flow depth and sediment discharge in open channels. *California Institute of Technology, W. M. Keck Laboratory of Hydraulics and Water Resources, Report*, p. 150–199. <https://authors.library.caltech.edu/25957/1/TR000108.pdf>
- CCNR. (2020). *Annual report, Inland navigation in Europe, Market observation*. https://www.ccr-zkr.org/files/documents/om/om20_ll_en.pdf
- CCR. (2021, May 1). *Information about the Rhine as waterway*. Website. <https://www.ccr-zkr.org/12030100-nl.html>
- CIRIA. (2007). *The Rock Manual: Physical processes and design tools*. Report C683. <https://www.kennisbank-waterbouw.nl/DesignCodes/rockmanual/>
- Copernicus. (2020). Flowing low: how can Europe use climate information to manage dry river spells? *Euronews*. <https://www.euronews.com/2020/08/03/flowing-low-how-can-europe-use-climate-information-to-manage-dry-river-spells>
- Deltares. (2021). *D-Morphology, 1D/2D/3D, User manual*. https://content.oss.deltares.nl/delft3d/manuals/D-Morphology_User_Manual.pdf
- Dorst, K., Meys, D. J., Schroevers, M., & Verheij, H. J. (2016). Prototype measuring of erosion and currents under the keel of a sailing ship in a canal. *Scour and Erosion - Proceedings of the 8th International Conference on Scour and Erosion, ICSE 2016*. <https://doi.org/10.1201/9781315375045-92>
- Earle, S. (2015). *Physical geology (2nd ed.) (ISBN: 978-1-77420-028-5)*. Victoria, B.C.: BCcampus. <https://opentextbc.ca/physicalgeology2ed/chapter/13-3-stream-erosion-and-deposition/>
- Ferguson, R. I., & Church, M. (2004). A simple universal equation for grain settling velocity. *Journal of Sedimentary Research*, 74(6), p. 933–937. <https://doi.org/10.1306/051204740933>
- Government of the Netherlands. (2021, January 4). *Ministry of Infrastructure and Water Management*. Website. <https://www.government.nl/ministries/ministry-of-infrastructure-and-water-management>

- Gutierrez, R. R., Abad, J. D., Parsons, D. R., & Best, J. L. (2013). Discrimination of bed form scales using robust spline filters and wavelet transforms: Methods and application to synthetic signals and bed forms of the Río Paraná, Argentina. *Journal of Geophysical Research: Earth Surface*, 118(3), p. 1400–1418. <https://doi.org/10.1002/jgrf.20102>
- Gutierrez, R. R., Mallma, J. A., Núñez-González, F., Link, O., & Abad, J. D. (2018). Bedforms-ATM, an open source software to analyze the scale-based hierarchies and dimensionality of natural bed forms. *SoftwareX*, 7, p. 184–189. <https://doi.org/10.1016/j.softx.2018.06.001>
- Hendrikssen, M. (2018). *Long-term morphologic development and the effect on hydraulic load* Master's Thesis, Delft University of Technology, Delft. <https://repository.tudelft.nl/islandora/object/uuid%3A3c55523f-f178-438c-8d05-33b9c03cfd2a?collection=education>
- IRM team. (2021, March 19). *Programma onder de omgevingswet (PoW)*. Website. <https://www.bouwplaatsirm.nl/programma-onder-de-omgevingswet-pow#no-back>
- Jing.fm. (2021, April 6). *Boat Clipart Transportation - Container Ship Icon Png* [Image]. <https://www.cleanpng.com/free/container-ship.html>
- Jonkeren, O., Ommeren, J. van, & Rietveld, P. (2008). *Effects of low water levels on the river Rhine on the inland waterway transport sector*. In *Economics and Management of Climate Change* (pp. 53–64). Springer New York. https://doi.org/10.1007/978-0-387-77353-7_5
- Julien, P. Y., Klaassen, G. J., Ten Brinke, W. B. M., & Wilbers, A. W. E. (2002). Case Study: Bed Resistance of Rhine River during 1998 Flood. *Journal of Hydraulic Engineering*, 128(12), p. 1042–1050. [https://doi.org/10.1061/\(asce\)0733-9429\(2002\)128:12\(1042\)](https://doi.org/10.1061/(asce)0733-9429(2002)128:12(1042))
- Lancia, L. (2014). *A survey of methods for analysis of the temporal evolution of speech articulator trajectories* [Image]. https://www.researchgate.net/figure/Shape-of-the-complex-Morlet-wavelet-used-as-a-mother-wavelet-for-the-analysis-described_fig5_261099505
- Lenselink, R. J. (2011). *Interaction between loaded barges and bed material*. Master's Thesis, Delft University of Technology, Delft. <http://resolver.tudelft.nl/uuid:75068a71-57fa-4fea-bb0f-9c39b4215f0d>
- Liu, Y., Liang, X. S., & Weisberg, R. H. (2007). Rectification of the Bias in the Wavelet Power Spectrum. *Journal of Atmospheric and Oceanic Technology*, 24(12), p. 2093–2102. https://journals.ametsoc.org/view/journals/atot/24/12/2007jtecho511_1.xml
- Lokin, L. R. (2020). *Dune dynamics under high and low flows: Literature report*. CE&M Research report; No. 2020R-003/WEM-003. University of Twente. <https://research.utwente.nl/en/publications/dune-dynamics-under-high-and-low-flows-literature-report>
- Lokin, L. R., Warmink, J. J., Bomers, A., & Hulscher, S. J. M. H. (2021). *The evolution of primary dunes during low flows on the Waal river*. In *Abstract from NCR Days 2021* (pp. 62–63). https://ris.utwente.nl/ws/portalfiles/portal/250865362/abstract_62_63.pdf
- Lokin, L. R., Warmink, J. J., Bomers, A. & Hulscher, S. J. M. H. (in prep.). *River dune dynamics during low flow*. Unpublished manuscript. Engineering Technology, University of Twente.
- Martin, W., & Boerop, L. (2019, January 24). Hoe het lage waterpeil van de Rijn een economische dip veroorzaakte in Duitsland – en ook de Nederlandse bouw raakte. *Business Insider*. <https://www.businessinsider.nl/hoe-het-lage-waterpeil-van-de-rijn-een-economische-dip-veroorzaakte-in-duitsland-en-ook-de-nederlandse-bouw-raakte/>

- Naqshband, S., Hoitink, A. J. F., McElroy, B., Hurther, D., & Hulscher, S. J. M. H. (2017). A Sharp View on River Dune Transition to Upper Stage Plane Bed. *Geophysical Research Letters*, 44(22), p. 437–444. <https://doi.org/10.1002/2017GL075906>
- Niemann, S. L., Fredsøe, J., & Jacobsen, N. G. (2011). Sand Dunes in Steady Flow at Low Froude Numbers: Dune Height Evolution and Flow Resistance. *Journal of Hydraulic Engineering*, 137(1), p. 5–14. <https://doi.org/10.1061/?ASCE?HY.1943-7900.0000255>
- Paarlberg, A. J., Dohmen-Janssen, C. M., Hulscher, S. J. M. H., Termes, P., & Schielen, R. (2010). Modelling the effect of time-dependent river dune evolution on bed roughness and stage. *Earth Surface Processes and Landforms*, 35(15), p. 1854–1866. <https://doi.org/10.1002/esp.2074>
- Reeze, B., van Winden, A., Postma, J., Pot, R., Hop, J., & Liefveld, W. (2017). *Watersysteemrapportage Rijntakken 1990-2015*. Ontwikkelingen waterkwaliteit en ecologie. Bart Reeze Water & Ecologie, Harderwijk. <https://www.stroming.nl/sites/default/files/2017-06/watersysteemrapportage-rijntakken-1990-2015.pdf>
- Rijkswaterstaat. (2021, January 4). *AIS: verkeersinformatie scheepvaart*. Website. <https://www.rijkswaterstaat.nl/zakelijk/verkeersmanagement/scheepvaart/scheepvaartverkeersbegeleiding/river-information-services/automatic-identification-system>
- Rijkswaterstaat. (2018, August 5). *Betrekkinglijnen Rijn*. Website. <https://www.helpdeskwater.nl/onderwerpen/waterveiligheid/primaire/beoordelen/@245949/betrekkinglijnen-rijn/>
- Rijkswaterstaat ON. (2018, January 4). *Viewer Waterdiepte kaarten Rijntakken RWS Oost-Nederland*. Website. https://maps.rijkswaterstaat.nl/gwproj55/index.html?viewer=ON_Waterdieptekaarten_Rijntakken
- Rivieren Nederland. (2021, July 29). *Grote rivieren Nederland*. Website. <http://www.rivierenederland.nl/grote-rivieren-nederland/>
- Robijns, T. (2014). *Flow beneath inland navigation vessels*. Master's Thesis, Delft University of Technology, Delft. <https://repository.tudelft.nl/islandora/object/uuid%3A380ca986-dccd-469b-94f6-7e57940ced4f>
- Ruijscher, T. V. de, Naqshband, S., & Hoitink, A. J. F. (2020). Effect of non-migrating bars on dune dynamics in a lowland river. *Earth Surface Processes and Landforms*, 45, p. 1361–1375. <https://doi.org/10.1002/esp.4807>
- Samann, F., & Schanze, T. (2019). An efficient ECG Denoising method using Discrete Wavelet with Savitzky-Golay filter. *Current Directions in Biomedical Engineering*, 5(1), p. 385–388. <https://doi.org/10.1515/cdbme-2019-0097>
- Schiereck, G. J. (1993). *Introduction to bed, bank, shore protection (ISBN: 9789065624413)*. p. 1.4, 4.1-4.11. TU Delft, Department Hydraulic Engineering, Delft, The Netherlands. <http://resolver.tudelft.nl/uuid:8341e6f2-5582-4920-8b7d-9e037f090a96>
- Shields, A. (1936). *Anwendung der Aehnlichkeitsmechanik und der Turbulenzforschung auf die Geschiebebewegung*. Doktor-Ingenieurs dissertation, Technischen Hochschule, Berlin. <https://repository.tudelft.nl/islandora/object/uuid%3A61a19716-a994-4942-9906-f680eb9952d6>

- Shinohara, K., & Tsubaki, T. (1959). On the characteristics of sand waves formed upon the beds of the open channels and rivers. *Reports of Research Institute for Applied Mechanics, Kyushu University, Japan*, 7, p. 15–45. <https://www.worldcat.org/title/on-the-characteristics-of-sand-waves-formed-upon-the-beds-of-the-open-channels-and-rivers/oclc/42756172>
- Sieben, J. (2009). Sediment management in the Dutch rhine branches. *International Journal of River Basin Management*, 7(1), p. 43–53. <https://doi.org/10.1080/15715124.2009.9635369>
- Steel, T. (2020, May 1). Duitse industrie snakt naar water. *De Tijd*. <https://www.tijd.be/politiek-economie/europa/economie/duitse-industrie-snakt-naar-water/10224558.html>
- Ten Brinke, W. B. M., Kruyt, N. M., Kroon, A., & Van Den Berg, J. H. (1999). *Erosion of sediments between groynes in the River Waal as a result of navigation traffic*. Spec. Publs int. Ass. Sediment, 28, pp. 147-160. <https://doi.org/10.1002/9781444304213.ch11>
- Ten Brinke, W. B. M., Wilbers, A. W. E., & Wesseling, C. (1999). Dune Growth, Decay and Migration Rates during a Large-Magnitude Flood at a Sand and Mixed Sand-Gravel Bed in the Dutch Rhine River System. Spec. Publs int. Ass. Sediment, 28, pp. 15-32. <https://doi.org/10.1002/9781444304213.ch2>
- Ten Brinke, W. B. M., Schulze, F. H., & van der Veer, P. (2004). Sand exchange between groyne-field beaches and the navigation channel of the Dutch Rhine: The impact of navigation versus river flow. *River Research and Applications*, 20, p. 899–928. <https://doi.org/10.1002/rra.809>
- Torrence, C., & Compo, G. P. (1998). A Practical Guide to Wavelet Analysis. *Bulletin of the American Meteorological Society*, 79(1), p. 61–78. [https://doi.org/10.1175/1520-0477\(1998\)079%3C0061:APGTWA%3E2.0.CO;2](https://doi.org/10.1175/1520-0477(1998)079%3C0061:APGTWA%3E2.0.CO;2)
- UNECE. (2012, January 4). *Map of the European Inland Waterway Network*. Website. https://unece.org/DAM/trans/main/sc3/European_inland_waterways_-_2012.pdf
- van den Berg, J. H., & van Gelder, A. (1993). Prediction of suspended bed material transport in flows over silt and very fine sand. *Water Resources Research*, 29(5), p. 1393–1404. <https://doi.org/10.1029/92WR02654>
- van der Mark, C. F., Blom, A., & Hulscher, S. M. J. H. (2008). Quantification of variability in bedform geometry. *Journal of Geophysical Research: Earth Surface*, 113(3), p. 1–11. <https://doi.org/10.1029/2007JF000940>
- Van Elk, E. (2018, October 24). The Waal at Boven-Leeuwen. *De Gelderlander*. <https://www.gelderlander.nl/nijmegen/benzeen-lozen-op-de-rijn-en-waal-zo-groot-is-het-probleem-en-dit-doen-de-overheden-eraan~a8e6e5c9/134566358/>
- van Rijn, L. C. (1984a). Sediment Transport, Part I: Bed Load Transport. *Journal of Hydraulic Engineering*, 110(10), p. 1431–1456. [https://doi.org/10.1061/\(ASCE\)0733-9429\(1984\)110:10\(1431\)](https://doi.org/10.1061/(ASCE)0733-9429(1984)110:10(1431))
- van Rijn, L. C. (1984b). Sediment Transport, Part II: Suspended Load Transport. *Journal of Hydraulic Engineering*, 10(11). [https://doi.org/10.1061/\(asce\)0733-9429\(1984\)110:11\(1613\)](https://doi.org/10.1061/(asce)0733-9429(1984)110:11(1613))
- van Rijn, L. C. (1984c). Sediment Transport, Part III: Bed forms and Alluvial Roughness. *Journal of Hydraulic Engineering*, 110(12), p. 1733–1754. [https://doi.org/10.1061/\(asce\)0733-9429\(1984\)110:12\(1733\)](https://doi.org/10.1061/(asce)0733-9429(1984)110:12(1733))
- van Rijn, L. C. (1993). *Principles of Sediment Transport in Rivers, Estuaries and Coastal Seas (ISBN 90-800356-2-9)*. Aqua Publications, Amsterdam, The Netherlands. <https://www.aquapublications.nl/Contentsbook2part2.pdf>

- Verheij, H. J., Stolker, C., & Groenveld, R. (2008). Inland waterways: Ports, waterways and inland navigation. VSSD, Delft, The Netherlands. <https://www.vssdshop.nl/product/f032lid/>
- Voogt, L., van Rijn, L. C., & Berg, J. H. van den. (1991). Sediment Transport of Fine Sands at High Velocities. *Journal of Hydraulic Engineering*, 117(7), p. 869–890. [https://doi.org/10.1061/\(asce\)0733-9429\(1991\)117:7\(869\)](https://doi.org/10.1061/(asce)0733-9429(1991)117:7(869))
- Wilbers, A. W. E. (2003). The development and hydraulic roughness of subaqueous dunes (ISSN 0169-4839). In *Nederlandse Geografische Studies*, (Issue 323). PhD Thesis, Universiteit Utrecht, Utrecht, The Netherlands. <http://resolver.tudelft.nl/uuid:2eca464c-6d9a-44e7-ba00-90bf342691ec>
- Wilbers, A. W. E., & Ten Brinke, W. B. M. (2003). The response of subaqueous dunes to floods in sand and gravel bed reaches of the Dutch Rhine. *Sedimentology*, 50(6), p. 1013–1034. <https://doi.org/10.1046/j.1365-3091.2003.00585.x>
- Wolters, M. A., Dasburg-Tromp, N. J. D. V., & Weekhout-Gunsing, R. F. E. (2020). *Klimaatbestendige Netwerken: Stresstest Hoofdvaarwegennet - Deelrapport Droogte* [Intern report].
- Ylla Arbós, C., Blom, A., Viparelli, E., Reneerkens, M., Frings, R. M., & Schielen, R. M. J. (2020). River Response to Anthropogenic Modification: Channel Steepening and Gravel Front Fading in an Incising River. *Geophysical Research Letters*, 48, p. 1–10. <https://doi.org/10.1029/2020GL091338>
- Zomer, J. Y., Naqshband, S., Vermeulen, B., & Hoitink, A. J. F. (2021). Rapidly Migrating Secondary Bedforms Can Persist on the Lee of Slowly Migrating Primary River Dunes. *JGR Earth Surface*, 126(3), p. 1–20. <https://agupubs.onlinelibrary.wiley.com/doi/full/10.1029/2020JF005918>

Appendices

A. Sediment transport induced by navigation

Table 9: List of parameters for an average situation in the Waal between Nijmegen and Zaltbommel (*italic parameters are determined below*).

Parameter	Description	Value	Unit	Source
A_s/A_c	Cross-section ratio between ship/channel	0.11	-	(Verheij et al., 2008)
B_s	Width of the ship	22.80	m	(Lenselink, 2011)
C	Chézy coefficient	47	$m^{1/2}/s$	(Lenselink, 2011)
C_{90}	<i>Grain related Chézy coefficient</i>	70.31	$m^{1/2}/s$	(van Rijn, 1984a)
D_{50}	Average grain size diameter	0.0023	m	(Verbeek, 2021) ⁷
D_{90}	90 th percentiles of the grain size distribution	0.0076	m	(Verbeek, 2021) ⁷
D_*	<i>Dimensionless particle parameter</i>	58.18	-	(van Rijn, 1984a)
g	Gravitational acceleration	9.81	m/s^2	-
h	Water depth	5.1	m	(Lenselink, 2011)
P	Rouse number	13.27	-	(Lenselink, 2011)
S_b	Bedload transport	Varying	kg/ms	(Deltares, 2021)
T	Bedshear parameter	Varying	-	(van Rijn, 1984a)
T_{nav}	Passage time ship	60	s	(Lenselink, 2011)
u_*	Shear velocity	$3.86 * 10^{-2}$	m/s	(Lenselink, 2011)
U	Velocity	1.1	m/s	(Lenselink, 2011)
U_r	Return current	0.39	m/s	(Verheij et al., 2008)
V	Volume sediment	Varying	m^3	(Lenselink, 2011)
V_s	Sailing speed	2.56	m/s	(Lenselink, 2011)
w_s	Settling velocity	0.21	m/s	(Ferguson & Church, 2004)
Δ	Relative density	1.65	-	-
κ	von Kármán constant	0.41	-	(Lenselink, 2011)
τ_b	Bed shear stress	Varying	kg/ms^2	(Lenselink, 2011)
$\tau_{b cr}$	Critical bed shear stress	1.49	kg/ms^2	(Deltares, 2021)
τ'_b	Bed shear stress related to grain roughness	Varying	kg/ms^2	(van Rijn, 1984a)
ν	Kinematic viscosity	10^{-6}	m^2/s	-
$\rho_{sed on bed}$	Specific mass of sediment on river bed	1073	kg/m^3	(Lenselink, 2011)
ρ_w	Density of water	1000	kg/m^3	-
θ_{cr}	Critical Shields parameter	0.04	-	(van Rijn, 1984a)

Type of transport

$$P = \frac{w_s}{\kappa * u_*} = 13.27 \rightarrow \text{bed load transport} \quad (11)$$

$$w_s = 1.1 \sqrt{\Delta g D_{50}} = 0.21 \text{ m/s}$$

$$u_* = \sqrt{\frac{\tau_b}{\rho}} = 3.86 * 10^{-2} \text{ m/s}$$

Bed load transport by navigation

$$S_{b,nav} = 0.1 \sqrt{\Delta g D_{50}^3 D_*^{-0.3} T^{1.5}} = 1.42 * 10^{-4} \text{ kg/ms} \quad (12)$$

⁷ (Verbeek, personal communication, August 3, 2021)

$$\begin{aligned}
D_* &= \left(\frac{\Delta g}{v^2}\right)^{\frac{1}{3}} D_{50} = \mathbf{58.18} \\
U_r &= 0.39 \text{ m/s} \rightarrow \frac{(V_s + U_r)^2 - V_s^2}{2gh} - \frac{U_r}{V_s + U_r} + \frac{A_s}{A_c} \\
\tau_b &= \left(\frac{(V_s + U_r)\sqrt{g}}{C}\right)^2 * \rho = 38.65 \text{ kg/ms}^2 \\
\tau'_b &= \left(\frac{C}{C_{90}}\right)^2 \tau_b = \left(\frac{C}{18 \log\left(\frac{12h}{D_{90}}\right)}\right)^2 \tau_b = 17.27 \text{ kg/ms}^2 \\
\theta_{cr} &= 0.013D_*^{0.29} = 0.04 \\
\tau_{b cr} &= \rho_w \Delta g D_{50} \theta_{cr} = 1.49 \frac{\text{kg}}{\text{ms}^2} \\
T &= \frac{\tau'_b - \tau_{b cr}}{\tau_{b cr}} = \frac{17.27 - 1.49}{1.49} = \mathbf{10.59} \\
V_{nav} &= \frac{S_{b,nav} * B_s}{\rho_{sed \text{ on bed}}} * T_{nav} = \mathbf{1.81 * 10^{-4} m^3} \tag{13}
\end{aligned}$$

Bed load transport by natural flow

$$\begin{aligned}
S_{b,nat} &= 0.1 \sqrt{\Delta g D_{50}^3 D_*^{-0.3} T^{1.5}} = \mathbf{1.67 * 10^{-5} kg/ms} \tag{14} \\
D_* &= \left(\frac{\Delta g}{v^2}\right)^{\frac{1}{3}} D_{50} = \mathbf{58.18} \\
\tau_b &= \left(\frac{U\sqrt{g}}{C}\right)^2 * \rho = 5.37 \text{ kg/ms}^2 \\
\tau'_b &= \left(\frac{C}{C_{90}}\right)^2 \tau_b = \left(\frac{C}{18 \log\left(\frac{12h}{D_{90}}\right)}\right)^2 \tau_b = 2.40 \text{ kg/ms}^2 \\
\theta_{cr} &= 0.013D_*^{0.29} = 0.04 \\
\tau_{b cr} &= \rho_w \Delta g D_{50} \theta_{cr} = 1.49 \frac{\text{kg}}{\text{ms}^2} \\
T &= \frac{\tau'_b - \tau_{b cr}}{\tau_{b cr}} = \frac{2.40 - 1.49}{1.49} = \mathbf{0.61} \\
V_{nat} &= \frac{S_{b,nat} * B_s}{\rho_{sed \text{ on bed}}} * T_{nav} = \mathbf{2.13 * 10^{-5} m^3} \tag{15}
\end{aligned}$$

B. Script Jupyter Notebook ship intensity analysis

Parquet converter

Steps to execute:

1. Load packages and define paths
2. Specify column names
3. Open JSON file
4. Define dataframe
5. Load JSON file into dataframe
6. Convert dataframe to Parquet file

0. Load packages:

```
In [ ]: from tqdm.notebook import tqdm
import os
import pytz
from datetime import datetime
import pandas as pd
import json
import time
from itertools import islice
```

0. Define paths

```
In [ ]: filename_json_in = '201910_output.json' # to adjust
filepath_json_in = '' # to fill in
json_in_file = os.path.join(filepath_json_in, filename_json_in)
filename_parquet_out = filename_json_in[:-5] + '.parquet'
filepath_parquet_out = '' # to fill in
parquet_out_file = os.path.join(filepath_parquet_out, filename_parquet_out)
```

1. Specify column names

```
In [ ]: cols = ['beam',
               'callsign',
               'cog',
               'cogValid',
               'courseQuality',
               'destination',
               'draughtInland',
               'draughtMarine',
               'eni',
               'eta',
               'heading',
               'headingQuality',
               'headingValid',
               'imo',
               'latitude',
               'length',
               'loaded',
               'longitude',
               'maneuver',
               'messageType',
               'mmsi',
               'name',
               'numberCrew',
               'objectType',
               'positionQuality',
               'positionValid',
               'raim',
               'rot',
               'rotValid',
               'seconds',
               'shiptypeERI',
               'shiptypeNMEA',
               'sog',
               'sogValid',
               'speedQuality',
               'timestampReceived',
               'timestampStatic',
               'timestampLast',
               'toBow',
               'toPort',
               'toStarboard',
               'toStern',
               'hazardousCargo',
               'shiptype',
               'numberPersonnel',
               'numberPassengers',
               'assigned',
               'nationality',
               'safetyAddressed',
               'safetyBroadcast']
```

2. Open JSON file

```
In [ ]: %%time
with open(json_in_file) as f:
    data = json.loads "[" +
        f.read().replace("{}\n{", "},\n{") + "]"
```

3. Define dataframe

```
In [ ]: %%time
row= range(0,len(data))
df_ship = pd.DataFrame(index=row, columns=cols)
```

4. Load JSON file into dataframe

```
In [ ]: %%time
z = 0
for k in tqdm(data):
    for l in k.values():
        for m in l:
            for n in m.keys():
                data_values = m[n]
                df_ship.at[z,n] = data_values
            z+=1
```

5. Convert dataframe to Parquet file

```
In [ ]: %%time
df_ship.to_parquet(parquet_out_file)
```

AIS data analysis

Steps to execute:

1. Load packages and define path
2. Read parquet file
3. Filter data set on position and outliers in navigation speed
4. Group data by MMSI-number
5. Convert AIS signals to ship track
6. Generalize ship track

0. Load packages:

```
In [ ]: import os
from tqdm.notebook import tqdm
from datetime import datetime, timedelta
import numpy as np
import pandas as pd
import movingpandas as mp
import geopandas as gpd
from geopandas import GeoDataFrame
import matplotlib.pyplot as plt
from shapely.geometry import Point, LineString, Polygon
import shapely.speedups
import hvplot.pandas
import hvplot.dask
from cartopy import crs as ccrs
import geoviews as gv
import geoviews.feature as gf
from geoviews import opts, tile_sources as gvts
gv.extension('bokeh', 'matplotlib')
import holoviews as hv
from holoviews import opts
from holoviews.operation import contours
hv.extension('bokeh')
from bokeh.plotting import figure, output_file, show
```

0. Define path

```
In [ ]: filename_parquet = '201910_output.parquet' # to adjust
filepath_parquet = '' # to fill in
parquet_file = os.path.join(filepath_parquet, filename_parquet)
```

1. Read parquet file and write to GeoDataFrame

Available information in data set:

- callsign: string
- **cog: double**
- cogValid: int64
- courseQuality: int64
- destination: string
- draughtInland: double
- draughtMarine: double
- eni: string
- eta: string
- heading: int64
- headingQuality: int64
- headingValid: int64
- imo: string
- **latitude: double**
- length: int64
- loaded: int64
- **longitude: double**
- maneuver: int64
- messageType: int64
- **mmsi: string**
- name: string
- numberCrew: int64
- objectType: string
- positionQuality: int64
- positionValid: int64
- raim: int64
- rot: double
- rotValid: int64
- seconds: int64
- **shiptypeERI: int64**
- shiptypeNMEA: int64
- **sog: double**
- sogValid: int64
- speedQuality: int64
- timestampReceived: string
- timestampStatic: string
- **timestampLast: string**
- toBow: int64
- toPort: int64
- toStarboard: int64
- toStern: int64
- hazardousCargo: int64
- **shiptype: string**
- numberPersonnel: int64
- numberPassengers: int64
- assigned: int64
- nationality: string
- safetyAddressed: string
- safetyBroadcast: null
- epfd: double

```
In [ ]: %%time
df = pd.read_parquet(parquet_file, columns=['timestampLast', 'mmsi', 'longitude', 'latitude', 'sog', 'cog', 'shiptype'])
df
```

```
In [ ]: %%time
df.replace(to_replace=[None], value=np.NaN, inplace=True) #Uniformity in data set
df['shiptypeERI'] = df['shiptypeERI'].apply(str)
df['shiptype'] = df['shiptype'].apply(str)
df['t'] = pd.to_datetime(df['timestampLast'], format="%Y-%m-%dT%H:%M:%SZ")
df = df.set_index('t') #Setting time as index
df
```

```
In [ ]: %%time
gdf = gpd.GeoDataFrame(
    df, geometry=gpd.points_from_xy(df.longitude, df.latitude), crs='EPSG:4326')
gdf
```

2. Filter data set on position and outliers in navigation speed

```
In [ ]: gdf.sog = gdf.sog * 1.852 # knots to km/hr
print("Original size: {} rows".format(len(gdf)))
gdf = gdf[gdf.sog<30]
print("Reduced to {} rows after removing abnormal high speed records".format(len(gdf)))
gdf = gdf[gdf.sog>0]
print("Reduced to {} rows after removing ships tracks with zero speed".format(len(gdf)))
```

```
In [ ]: print("GeoDataframe has {} rows".format(len(gdf)))

lat_point_list = [51.9, 51.902, 51.905, 51.905, 51.9]
lon_point_list = [5.54, 5.554, 5.554, 5.54, 5.54]

area_of_interest = Polygon(zip(lon_point_list, lat_point_list))
new_data = gdf.geometry.within(area_of_interest)
gdf['status'] = new_data
gdf.drop(gdf[gdf['status'] == True].index, inplace=True)
print("Reduced to {} rows".format(len(gdf)))

lat_point_list = [51.8975, 51.8975, 51.895, 51.895, 51.8975]
lon_point_list = [5.595, 5.605, 5.605, 5.595, 5.595]

area_of_interest = Polygon(zip(lon_point_list, lat_point_list))
new_data = gdf.geometry.within(area_of_interest)
gdf['status'] = new_data
gdf.drop(gdf[gdf['status'] == True].index, inplace=True)
print("Reduced to {} rows".format(len(gdf)))

lat_point_list = [51.901, 51.901, 51.904, 51.904, 51.901]
lon_point_list = [5.63, 5.64, 5.64, 5.63, 5.63]

area_of_interest = Polygon(zip(lon_point_list, lat_point_list))
new_data = gdf.geometry.within(area_of_interest)
gdf['status'] = new_data
gdf.drop(gdf[gdf['status'] == True].index, inplace=True)
print("Reduced to {} rows".format(len(gdf)))

lat_point_list = [51.899, 51.899, 51.907, 51.907, 51.899]
lon_point_list = [5.66, 5.68, 5.68, 5.66, 5.66]

area_of_interest = Polygon(zip(lon_point_list, lat_point_list))
new_data = gdf.geometry.within(area_of_interest)
gdf['status'] = new_data
gdf.drop(gdf[gdf['status'] == True].index, inplace=True)
print("Reduced to {} rows".format(len(gdf)))

lat_point_list = [51.894, 51.894, 51.884, 51.884, 51.894]
lon_point_list = [5.54, 5.68, 5.68, 5.54, 5.54]

area_of_interest = Polygon(zip(lon_point_list, lat_point_list))
new_data = gdf.geometry.within(area_of_interest)
gdf['status'] = new_data
gdf.drop(gdf[gdf['status'] == True].index, inplace=True)
print("Reduced to {} rows".format(len(gdf)))

lat_point_list = [51.898, 51.898, 51.893, 51.893, 51.898]
lon_point_list = [5.59, 5.637, 5.637, 5.59, 5.59]

area_of_interest = Polygon(zip(lon_point_list, lat_point_list))
new_data = gdf.geometry.within(area_of_interest)
gdf['status'] = new_data
gdf.drop(gdf[gdf['status'] == True].index, inplace=True)
print("Reduced to {} rows".format(len(gdf)))

lat_point_list = [51.897, 51.897, 51.884, 51.884, 51.897]
lon_point_list = [5.54, 5.56, 5.67, 5.54, 5.54]

area_of_interest = Polygon(zip(lon_point_list, lat_point_list))
new_data = gdf.geometry.within(area_of_interest)
gdf['status'] = new_data
gdf.drop(gdf[gdf['status'] == True].index, inplace=True)
print("Reduced to {} rows".format(len(gdf)))
```

```
In [ ]: gdf_up = gdf[gdf.cog<180]
print("{} rows of upsailing ships".format(len(gdf_up)))
gdf_down = gdf[gdf.cog>180]
print("{} rows of downsailing ships".format(len(gdf_down)))
```

3. Group data by MMSI-number

```
In [ ]: %%time
MIN_LENGTH = 100 # minimal length ship trajectory
traj_collection = mp.TrajectoryCollection(gdf, 'mmsi', min_length=MIN_LENGTH)
print("Finished creating {} trajectories".format(len(traj_collection)))
```

4. Convert AIS signals to ship track

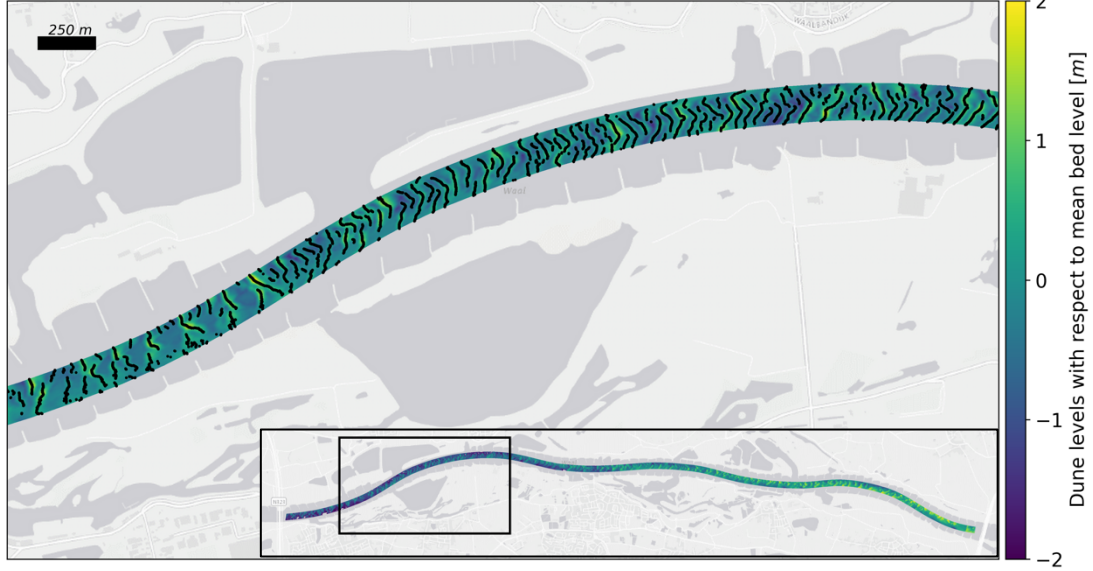
```
In [ ]: %%time
trips = mp.ObservationGapSplitter(traj_collection).split(gap=timedelta(minutes=5)) # split trajectory by time
print("Finished creating {} trajectories".format(len(trips)))
```

5. Generalize ship track

```
In [ ]: %%time
trips_gen = mp.MinDistanceGeneralizer(trips).generalize(tolerance=100) # generalize by resampling points every
# use '%store' to save variables
```

C. Dune pattern Waal section Beneden-Leeuwen

Dune pattern of the crests at the Waal section Beneden-Leeuwen for 17-03-2020



Dune pattern of the crests at the Waal section Beneden-Leeuwen for 07-08-2020

